İZMİR KÂTİP ÇELEBİ ÜNİVERSİTESİ
2010
GRADUATE SCHOOL OF NATURAL AND APPLIED SCIENCES

Exhaust Thermal Energy Recuperation in Small Gas Turbine and Turbojet Engines

Submitted to the Graduate School of Natural and Applied Sciences
in partial fulfillment of the requirements for the degree of

Master of Science

in Mechanical Engineering

by

Deniz Hakyemez Çetiner

ORCID 0000-0002-5279-9235

January, 2022

This is to certify that we have read the thesis **Exhaust Thermal Energy Recuperation in Small Gas Turbine and Turbojet Engines** submitted by **Deniz Hakyemez Çetiner**, and it has been judged to be successful, in scope and in quality, at the defense exam and accepted by our jury as a MASTER'S THESIS.

APPROVED BY:

Advisor: **Assoc. Prof. Dr. Sercan Acarer**
İzmir Kâtip Çelebi University

Committee Members:

Assoc. Prof. Dr. Sercan Acarer
İzmir Kâtip Çelebi University

Assoc. Prof. Dr. Mehmet Akif Ezan
Dokuz Eylul University

Assoc. Prof. Dr. Ziya Haktan Karadeniz
İzmir Kâtip Çelebi University

Date of Defense: December 29, 2021

Declaration of Authorship

I, **Deniz Hakyemez Çetiner**, declare that this thesis titled **Exhaust Thermal Energy Recuperation in Small Gas Turbine and Turbojet Engines** and the work presented in it are my own. I confirm that:

- This work was done wholly or mainly while in candidature for the Master's degree at this university.
- Where any part of this thesis has previously been submitted for a degree or any other qualification at this university or any other institution, this has been clearly stated.
- Where I have consulted the published work of others, this is always clearly attributed.
- Where I have quoted from the work of others, the source is always given. This thesis is entirely my own work, with the exception of such quotations.
- I have acknowledged all major sources of assistance.
- Where the thesis is based on work done by myself jointly with others, I have made clear exactly what was done by others and what I have contributed myself.

Signature:

Date: 10.01.2022

Exhaust Thermal Energy Recuperation in Small Gas Turbine and Turbojet Engines

Abstract

Efforts to reduce carbon dioxide emissions, which come into prominence with the increasing air pollution day by day, continue in every field. In areas such as electricity generation and transportation, which constitute the majority of air pollution, the use of gas turbines is common. The subject of this thesis, recuperator design is one of the methods studied to increase efficiency and save fuel with these engines that are open to improvement. The shell and tube heat exchanger for two different micro gas turbine engines, land and aero, has been modeled by considering pressure loss and temperature rise. Due to area limitations in aero engines, a more complex design has been considered for the land engine. The recuperator with two main sections leaf and manifold analyzed in 2D and 3D. By optimizing the design using the ANSYS DOE program, it is aimed to obtain the most efficient model for land and aero type microturbines. In addition to these, thermodynamic cycle analysis has been performed by using component performance maps according to CFD analysis. As a result of these studies using the matching method, the threshold effectiveness that will provide zero benefits for the engine has been calculated. Thus, the ratio of the efficiency of the heat exchanger to the threshold value became a distinctive parameter. To sum up, improvements have been observed as 2.54% and 4.82% less TSFC of land and aero engines when the fuel mass flow rates and thrust forces of the most efficient models have been compared with the engine without a recuperator.

Keywords: Micro gas turbine, recupertor, effectiveness

Küçük Gaz Türbini ve Turbojet Motorlarında Egzoz Termal Enerji Geri Kazanımı

Öz

Her geçen gün artan hava kirliliği ile önem kazanan karbondioksit emisyonunun azaltılmasına yönelik çalışmalar her alanda devam etmektedir. Elektrik üretimi, taşımacılık gibi hava kirliliğinin büyük kısmını oluşturan alanlarda gaz türbini kullanımı yaygındır. Gelişime açık bu motorlar ile verimi arttırmak ve yakıt tasarrufu sağlamak amacıyla çalışılan yöntemlerden biri olan reküperatör tasarımı bu tezin konusudur. Yer ve hava olmak üzere iki farklı mikro gas türbin motoru için borulu ısı değiştirici basınç kaybı ve sıcaklık artışı dikkate alınarak modellenmiştir. Hava tipi motorlarda alan kısıdı olmasından dolayı, yer tipi motor için daha karmaşık bir tasarım ele alınmıştır. Yaprak ve dağıtım boruları olmak üzere iki ana bölüme sahip olan reküperatörün 2B ve 3B HAD analizleri yapılmış. Tasarım ANSYS DOE programı kullanılarak optimize edilerek, yer ve hava tipi mikro türbinler için en verimli model elde etmek amaçlanmıştır. Bunlara ek olarak, HAD analiz sonuçlarına göre bileşen performans haritalarından faydalanarak termodinamik çevrim analizi yapılmıştır. Eşleşme yöntemi kullanılan bu çalışmaların sonucunda motor için sıfır fayda sağlayacak eşik etkinlik değeri hesaplanmıştır. Böylece ısı değiştiricinin sahip olduğu etkinliğin eşik değerine oranı ayırt edici bir parametre olmuştur. Sonuç olarak yapılan analizler karşılaştırılmış, en verimli modellerin yakıt kütlesel debileri ile itki kuvvetleri reküperatörsüz motorla kıyaslandığında yer ve hava tipi motorların özgül yakıt tüketiminde %2.54 ve %4.82 oranında iyileşmeler gözlenmiştir.

Anahtar Kelimeler: Mikro gaz türbin, reküperatör, etkinlik

To my precious mother,

Acknowledgment

First and foremost, I am grateful to my supervisor, Assoc. Prof. Dr. Sercan Acarer for his invaluable knowledge, kind help, and patience during my study. His support has encouraged me every time in both my academic and personal life. Also, I would like to thank Assoc. Prof. Dr. Beni Çukurel for his insightful comments and suggestions and Prof. Guillermo Paniagua, David Linsky, Michael Palman for their contributions. Additionally, I would like to express my gratitude to the NATO SPS program for giving me the opportunity to study this project and funding. Above all, I would like to extend my sincere thanks to my mother Gülhan Kaymak, and my husband Baha Çetiner. It would be tough for me to complete my study without their tremendous help and support. Finally, my appreciation also goes out to the rest of my family and friends for their encouragement all through my life.

Table of Contents

List of Figures

List of Tables

List of Abbreviations

ORCID	Open Researcher and Contributor ID
NATO	North Atlantic Treaty Organization
TSFC	Thrust-Specific Fuel Consumption

List of Symbols

D_h	Hydraulic Diameter [mm]
h	Heat Transfer Coefficient [$Wm^{-2}K^{-1}$]
k	Thermal Conductivity [$Wm^{-1}K^{-1}$]
q	Heat Transfer [W]
T	Temperature [K]
δ	Pressure Standard Constants
θ	Temperature Standard Constants
P	Presurre [Pa]
$\dot{m}$	Mass Flow Rate [kgs^{-1}]
f	Fuel to Air Mass Flow Rate
N	Rotational Speed [rev min^{-1}]
ΔH	Change of Enthalpy [J s^{-1}]
ρ	Density [kg m^{-3}]
R	Gas Constant [$Jkg^{-1}K^{-1}$]
Δs	Change of Entropy [$Jkg^{-1}K^{-1}$]
c_p	Specific Heat [$Jkg^{-1}K^{-1}$]
V	Speed [ms^{-1}]
z	Elevation [m]
c	Speed of Sound [ms^{-1}]
M	Mach Number
η	Efficiency
F_{thrust}	Thrust Force [N]

ε_t	Threshold Effectiveness
ε	Effectiveness

Chapter 1

Introduction

A gas turbine is an internal combustion engine that converts thermal energy produced by the combustion of fuel to mechanical power or propulsive thrust. These engines can be separated into 2 main parts, a gas generator, where the air is compressed and the air-fuel mixture is burnt to produce high thermal energy, and a power converter, which may be shaft work, gearbox, etc. As distinct from part 2, the first part consists of intake, compressor, combustion chamber, and turbine which produced shaft power for the compressor as shown in figure 1.1(a). Also, Figure 1.1(b) represents the simple Brayton cycle for gas turbines. This ideal cycle is an internally reversible process that has four-stage as isentropic compression (1-2), constant-pressure heat addition (2-3), isentropic expansion (3-4), constant-pressure heat rejection (4-1).

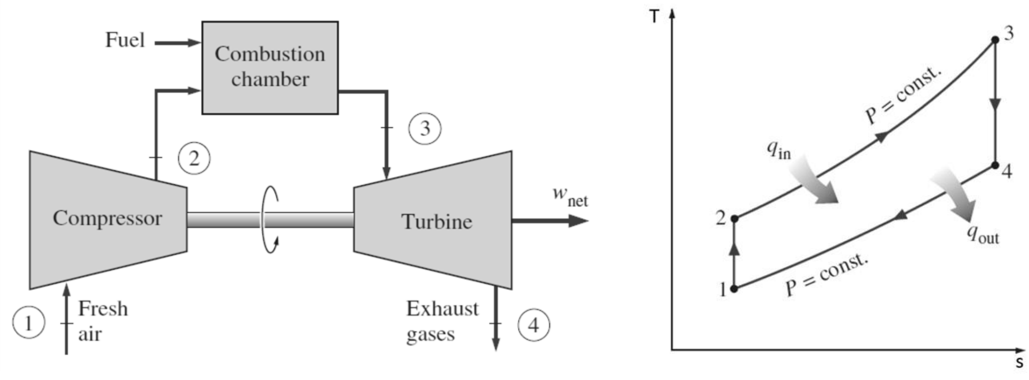

(a) (b)

Figure 1.1: A schematic diagram (a) and Brayton cycle (b) for a simple gas turbine engine [1]

Since the Second World War, gas turbine engines have attracted great interest and have been improved more and more. Owing to these technological developments and beneficial properties like compactness, high power/low weight ratio, various options about fuel types, gas turbines have a wide range of applications like military and commercial aviation, electrical generation, mechanical drive, marine power. Currently, it is mostly used in aviation commercial and military aircraft, helicopters and business jets. On the other hand, the engine's cost of production is considerable. Especially, recent years investments have increased and it continues day by day as shown in Figure 1.2.

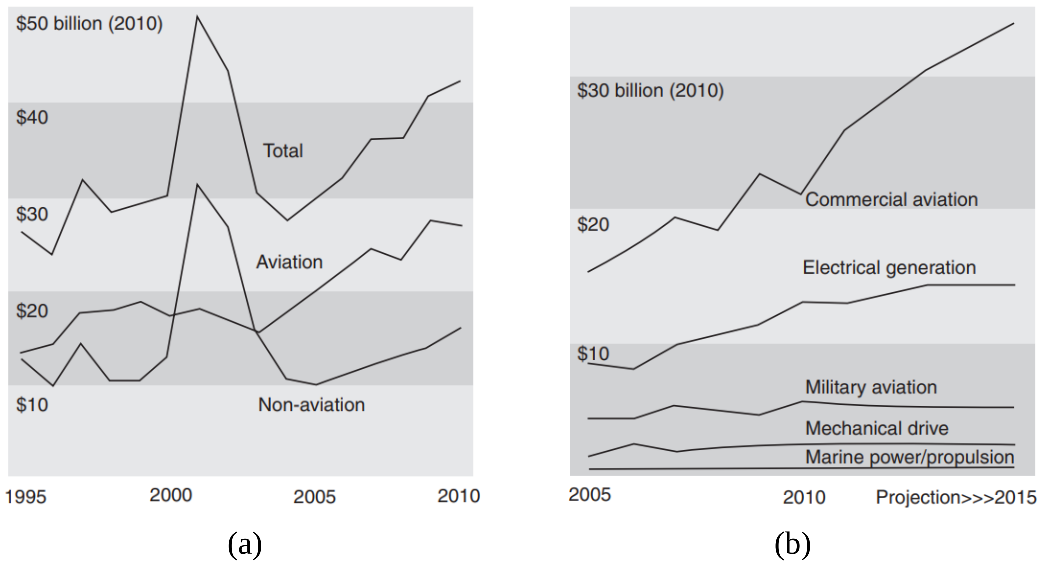

Figure 1.2: Global gas turbine production, (a) according to aviation, (b) different areas [2]

Gas turbines are classified into several types: Frame type heavy-duty gas turbines or industrial gas turbines, aircraft-derivative gas turbines, and micro gas turbines that may belong to the two former types as shown in figure 1.3 [3]. In this thesis, two types of micro gas turbines, land and aero engines, have been researched. These two engines are different from each other in terms of the principle of power transmission is different. While the power is produced via propulsion in aero-engines, there is a power turbine in addition to the turbine that runs the compressor and it is transmitted using a shaft.

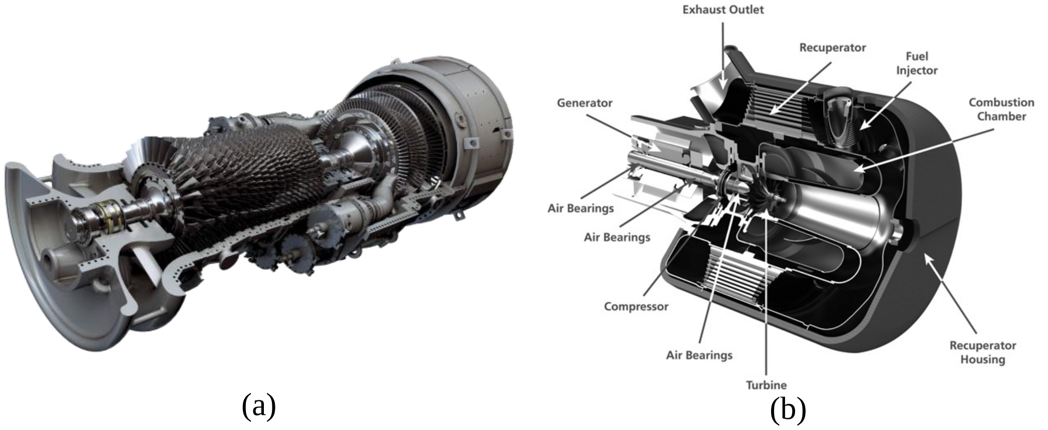

Figure 1.3: 7E.03 industrial gas turbines of General Electric (a) C65 microturbine of Capstone (b) [4,5]

Apart from all these, high carbon dioxide emission is a serious threat to our future, and according to the research conducted in 2010, fossil fuels used in electricity generation caused for 41%, transportation 23% and 17% for industrial uses of the CO_2 emissions [6]. Gas turbine engines used in all these sectors play a major role in reducing CO_2 emissions. Studies have focused on 2 main solutions: increasing efficiency and capturing CO_2 with a system. There are many methods used in gas turbines to increase efficiency and reduce fuel consumption such as intercooling, overall pressure ratio, water injection in the compressor, steam injection in the combustor and recuperation.

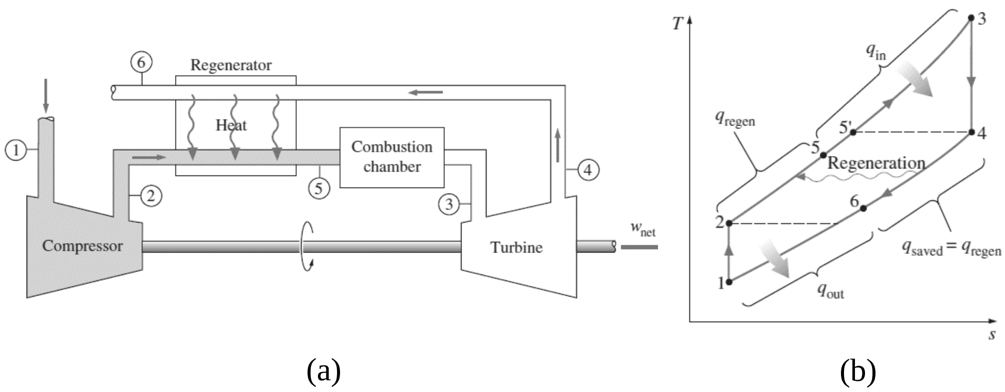

Figure 1.4: Schematic representation of regenerative gas turbine engine (a), T-s diagram of regenerative Brayton cycle (b) [1]

In this study, recuperation has been investigated as a method. Before speaking of the application areas of this method, its working principle should be mentioned briefly. As shown in Figure 1.4., basically recuperation in a gas turbine is preheating the air at the exit of compressor with using the thermal energy of exhaust air. In this way, the useful energy that is about to be exhausted is regained to the system. However, this method has a drawback such as causing a pressure drop. To sum up, when using recuperation, efficiency should increase but there should be no loss of thrust due to pressure drop [7].

Although, recently, using recuperation is common as additive technology, design criteria of a recuperator in aviation are more challengeable than in industrial areas. The importance of weight, area, and compactness in aero-engines is the main reason for this situation. Unlike these engines, land types have enough space and weight is not a problem as much as aviation.

In the late 1970s in Germany, the compact heat exchangers for micro gas turbine engines applications were started to study [8]. After these applications, improvements on the heat exchangers for microturbines were investigated such as higher efficiency, lower cost for manufacturing, developing new materials [9,10]. Antoine et al. have developed a spiral model by gaining a different point of view to the studies with regular designs such as circular cubes [11]. Moreover, these recuperators have been produced by Solar Turbines and Caterpillar since 1995 which is made from fully welded stainless steel, and since 2001 Capstone Turbine Corporation manufactures primary surface annular recuperators for microturbines using Solar Turbines license [12].

In this thesis, design optimizations of a shell and tube heat exchanger for land and aero micro gas turbine engines (positioned at the exhaust outlet) have been studied. Initially, the transition to 3-dimensional has been established with the best model from the 2-dimensional optimization analyzes. The results have been evaluated by two main parameters: temperature rise and pressure drop. Since the temperature increase will be associated with the effectiveness of the heat exchanger, the effectiveness ratio is taken into account in the results according to the increase in pressure drop. The increased pressure losses due to the heat exchanger positioned at the outlet must be compensated by high effectiveness. However, the pressure drops that change as a result of each new analysis cause a new effectiveness value to be determined to compensate. Hence, in this study, a thermodynamic cycle code has been developed using the MATLAB program to calculate the effectiveness that reduces the loss caused by pressure losses to zero benefits. With this code, besides calculating the required minimum effectiveness, it has been also intended to match the performance maps of the compressor and turbine. Thus, new operating points have been determined for each new pressure loss. In addition to all these, many different models have been designed to increase the current effectiveness of the recuperator. Internal fins have been optimized to enhance heat transfer while directing the flow. Likewise, outer fins have been added to the tube surface on the hot side, and the effectiveness value has been planned to be maximized. Eventually, the manifolds connecting the heat exchanger to other components are designed to fit the engine and minimize pressure loss.

Chapter 2

Methods

2.1 Computational Fluid Dynamics (CFD) Methods

Design of the heat exchanger for micro gas turbine engines has been researched as two main headings. Many investigations such as optimizing geometry of the recuperator, the analysis and comparison of different models have been studied by the Computational Fluid Dynamics (CFD) method, which is commonly used in gas turbine engine analysis. Moreover, various calculations have been obtained by developing a code to compare the analysis results and to examine them. The details of these thermodynamic calculations will be discussed in the following sections.

2.1.1 Design of the Heat Exchanger for Land Micro Gas Turbines

As mentioned above, the limitation of the field for Land Micro Gas Turbines is less than in aero engines. Consequently, a relatively larger engine diameter is used in this study. The design of the recuperator to be adapted to the engine has been started initially in the 2D plane. During modeling, pressure loss has been aimed to be minimized by using various optimization methods, and in 3D, computational fluid dynamics (CFD) analyzes have been done with the optimum geometry which has been obtained from optimization. The cross-sectional areas of the leaves, which are one of the 2 main parts of the recuperator, are modeled separately as straight and curved. Also, in the other main section, the manifolds' single and multiple pipe designs have been investigated. The optimum whole model has been compared with different leaf studies in terms of pressure loss-effectiveness values. Finally, the 3D CFD analyzes have been validated by mesh independence studies.

At the beginning, this design has been optimized with stochastic genetic algorithm. While the optimization method using the design of experiment (DOE) module of the ANSYS program, the flow routers called splitters have been constructed as well as modeling the main outer and inner lines of the pipe. Optimizing a single turn in the geometry of the recuperator, which consists of a total of 5 identical u-turns with the routers, has been initially sufficient. Optimization of a u-turn has consisted of two-part as main structure (figure 2.2a) and construction lines (figure 2.2b). The parameters to optimize splitters have been classified as r_0 to r_4 and each distance of lines between splitters represents an input parameter. Moreover, static temperature and pressure, and mass flow rate of the outlet are output parameters of optimization. Figure 2.3 shows the local sensitivities vs these output parameters according to inputs.

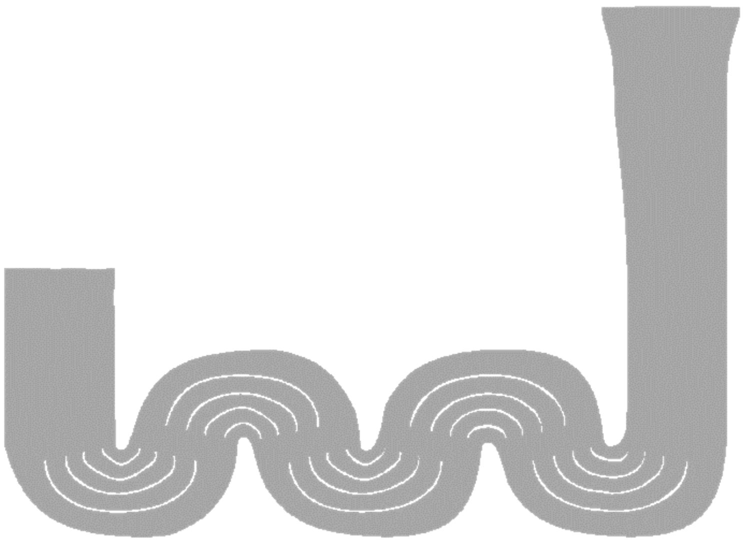

Figure 2.1: Design of the geometry in 2D

Afterward, the entire geometry reached as a result of optimization analysis using DOE, has been finally improved with using the method gradient-based adjoint optimizer. At the end of all these steps, the optimum design of 2D geometry has been obtained which shows in Figure 2.1.

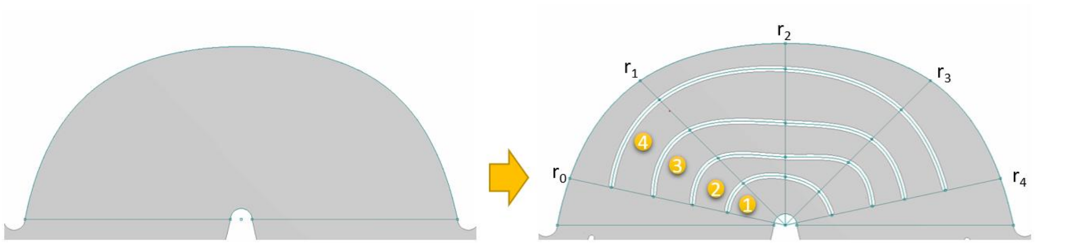

(a) (b)

Figure 2.2: Optimization parameters: (a) Main structure and (b) Construction lines

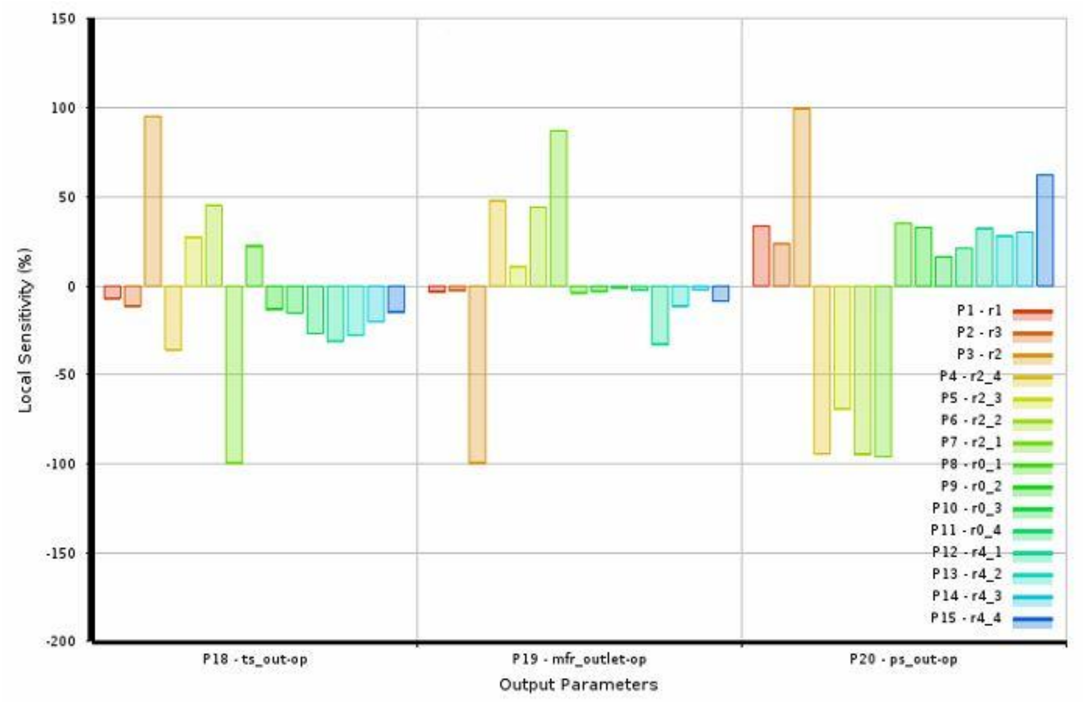

Figure 2.3: The graph of local sensitivity with respect to output parameters for each input

The modeled 2D geometry has been adapted to the 3D model. Many important parameters should be considered when transitioning to 3D modeling. The first of the parameters evaluated in this study is how the cross-sectional area of the tube section of the recuperator should be. Two different designs have been studied on the subject: straight and curved which are shown in Figure 2.4. CFD analyzes have been run under the same conditions, and the purpose was minimizing pressure drop, maximizing the effectiveness.

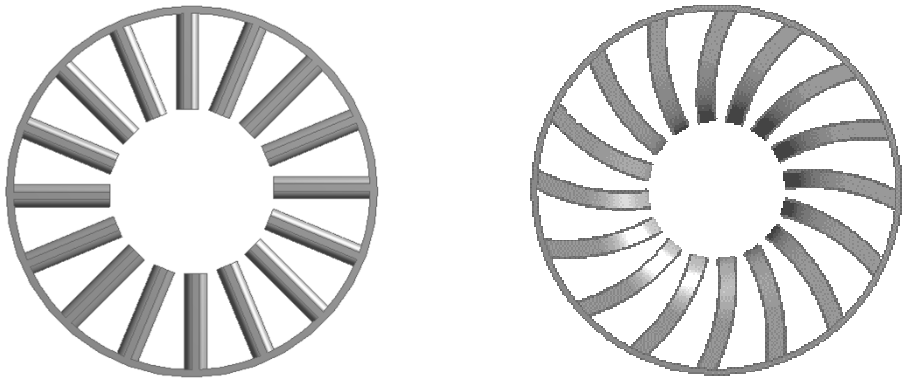

(a) (b)

Figure 2.4: Design of the geometry in 3D: Multiple U-bend body (a) Case 1, (b) Case 2

Problems such as flow separation that will occur in the design cause a high pressure drop. Therefore, besides the appropriate tube cross-sectional area, the manifold design is significant in terms of preventing pressure drop. The manifold, which is other part of the recuperator, provides that the relatively cold air coming out of the compressor is through to the heat exchanger, while it sends the hot air coming out of the heat exchanger to the combustion chamber. In this study, the pipes mentioned have been studied in 2 ways as single and multiple. In the first design, the cold air passing through the compressor is carried to the tubes with the help of a single pipe that surrounds the entire heat exchanger. Likewise, the hot air coming from the tubes is collected in a single outlet pipe and sent to the combustion chamber. In the other model studied, each tube has its own manifold and these multiple manifolds carry the air to the relevant sections. Figure 2.5 shows these different designs of the manifold.

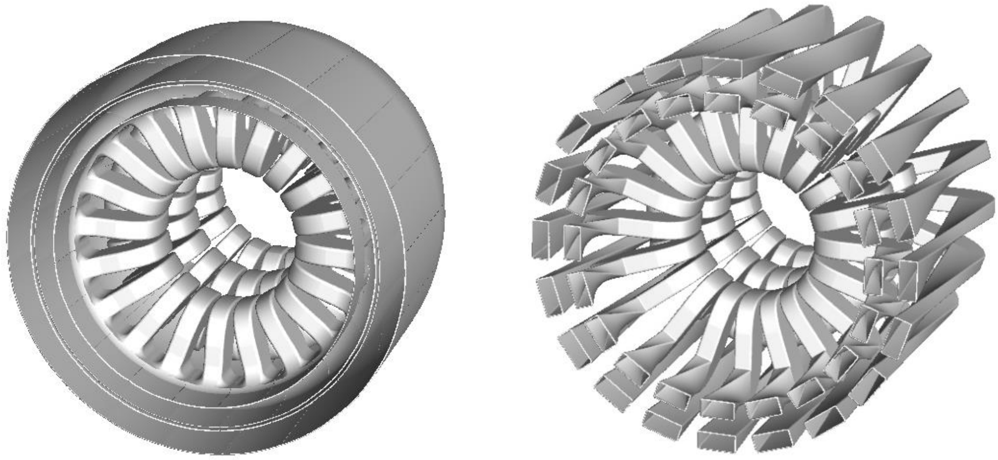
(a) (b)

Figure 2.5: Different design models of manifold: (a) Single pipe, (b) Multiple pipes

2.1.2 Design of the Heat Exchanger for Aero Micro Gas Turbines

Considering the potential flying application of the adaptive cycle engine, the recuperator design is a complex optimization problem involving minimizing weight and pressure drop while maximizing temperature recovery. As the solution of this problem, first of all, the cross-sectional area has been designed as in the land type. Unlike the first heat exchanger, multiple u-turns have been avoided in order to tolerate the restriction due to the diameter of the aero egine. For this reason, based on a single u-turn model, 3 different cross-sectional areas have been analyzed. In addition, the tube length is another major parameter. Moreover, in order to reduce pressure losses, the model has been improved by using leading-trading angles in the sections where flow separation occurs. External fins have been added to the geometry and figure 2.6 shows the final tube geometry, where pressure losses are minimized, in order to increase effectiveness. Eventually, the manifold has been designed by adapting it from the study [13].

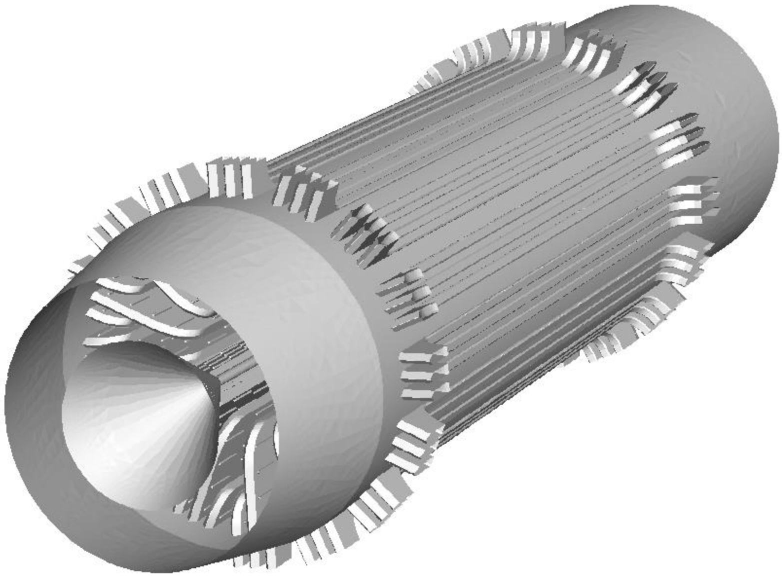

Figure 2.6: The geometry of the heat exchanger for aero gas turbines

The pressure loss must be low for both the hot and cold sides. Accordingly, it is aimed to find optimum geometry, and some parameters were taken into consideration while designing the recuperator. The one of them is the cross-sectional geometry of the tube in a leaf. Figure 2.7 shows three different cross-sectional models which are compared with respect to temperature rise and pressure loss. These models created by revolving (case 1), extending (case 2), and using multiple extended bodies (case 3). Case 1, which is shown in Figure 2.7(a), is designed by comparing different angles based on pressure and temperature. According to this angle comparison, the optimum revolved model is that the cold cross-sectional area is 40 percent of the total cross-sectional area. Unlike Case 1, case 2 is extended to leave enough space in the hot part as shown in Figure 2.7(b). However, this model has a lot of unused space. For this reason, 2 short and 1 long extended body are modeled in case 3 which is shown in Figure 2.7(c).

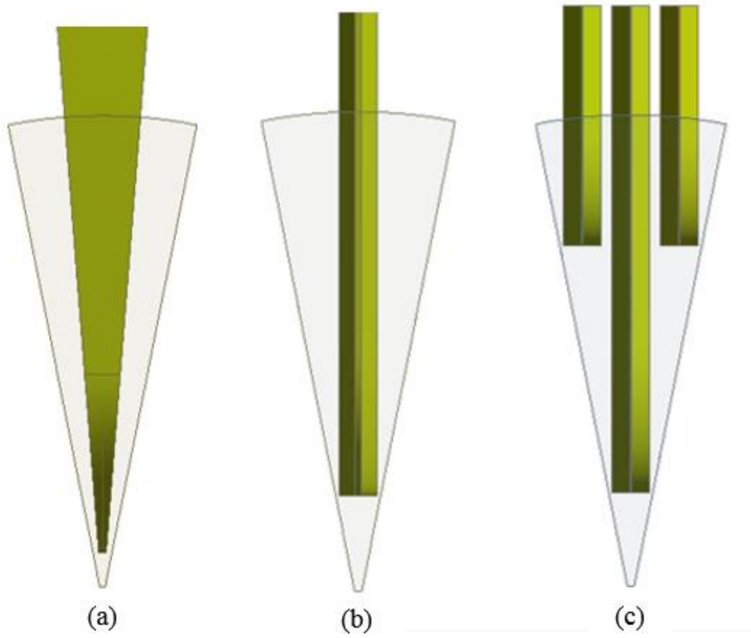

Figure 2.7: Cross-sectional models: (a) Case 1, (b) Case 2, (c) Case 3

Figure 2.8 shows that other parameters which are the length of the cold body (tube) and the angles of leading-trailing edges. Same as the cross-section, three different models are investigated in this parameter, which are two and three times a particular length. On the other hand, both the leading and trailing angles of the first model are 55 degrees. Moreover, the Second and third cases have respectively Leading Edge: 35° Trailing Edge: 15° and Leading Edge: 20° Trailing Edge: 6°.

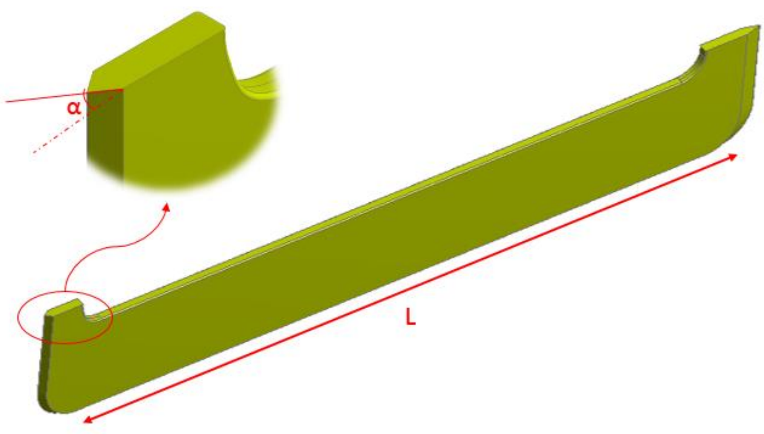

Figure 2.8: The length of the cold body and the angles of leading-trailing edges

Temperature is also a significant parameter for the recuperator study like pressure losses. Therefore, internal and external fins have been added to the design of the recuperator to enhance heat transfer. Several models for internal fin have been analyzed like short and close fin designs. However, the optimum number and density of fins for the inside of the cold side have been shown in figure 2.9 (a). Besides, the optimum model for external fins, which is shown in figure 2.9 (b), has been obtained closer and shorter than inside. The main reason for the difference is the effects of pressure losses on the hot and cold sides. Moreover, figure 2.9 (c) shows the axial view of a leaf including fins.

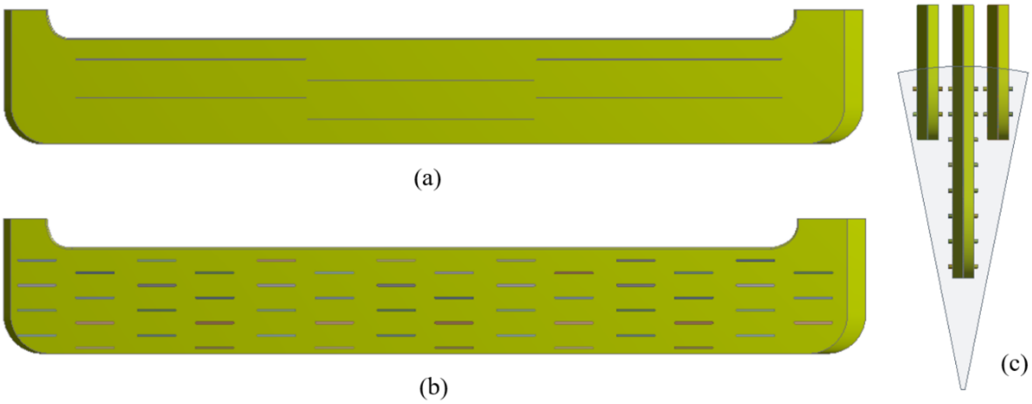

Figure 2.9: (a) Internal, (b) External fin models, (c) The axial view of a leaf with fins

In addition to these models, manifolds have been added to the recuperator and the design of manifold has been adapted from the study of Verstraete et al. [13]. The inlet and outlet manifold have been connected to the outlet of the compressor and inlet of the combustion chamber. The Inlet of the manifold has been designed with the same diameter as the compressor outlet because of connection. However, if the whole recuperator had the same diameter as the compressor, the pressure losses would increase too much and the u-turn design between the manifold and the cold body would not be possible. That's why the geometry with manifold has been designed as conical. Figure 2.10 shows a leaf with manifolds and figure 2.11 shows the whole recuperator geometry.

Figure 2.10: The view of cold body in a leaf with manifold

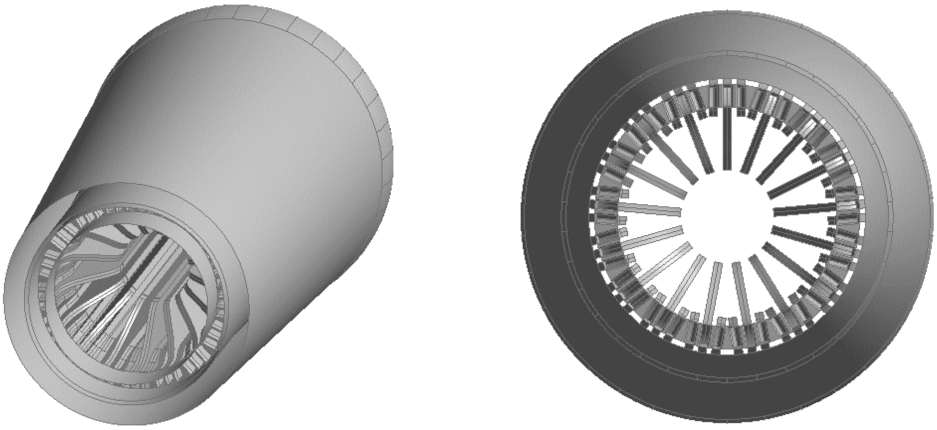

(a) (b)

Figure 2.11: (a) The isometric view, (b) The front view of recuperator with manifold

2.1.3 Mesh Independency

For simulation studies, since the mesh structure is significant for the accuracy of the results, the mesh independence study has been detailed in this part of the thesis as shown in figure 2.12. A total of six mesh models, three medium and three fine, with a relatively increasing number of elements, have been analyzed. Considering the two main parameters, temperature and pressure changes, six models have been compared in terms of consistency of the results. In addition to the accuracy of the temperature and pressure loss difference with the finest mesh in comparison, in order to prevent time waste, the coarsest model is the optimum one among the models in which the difference is minimal.

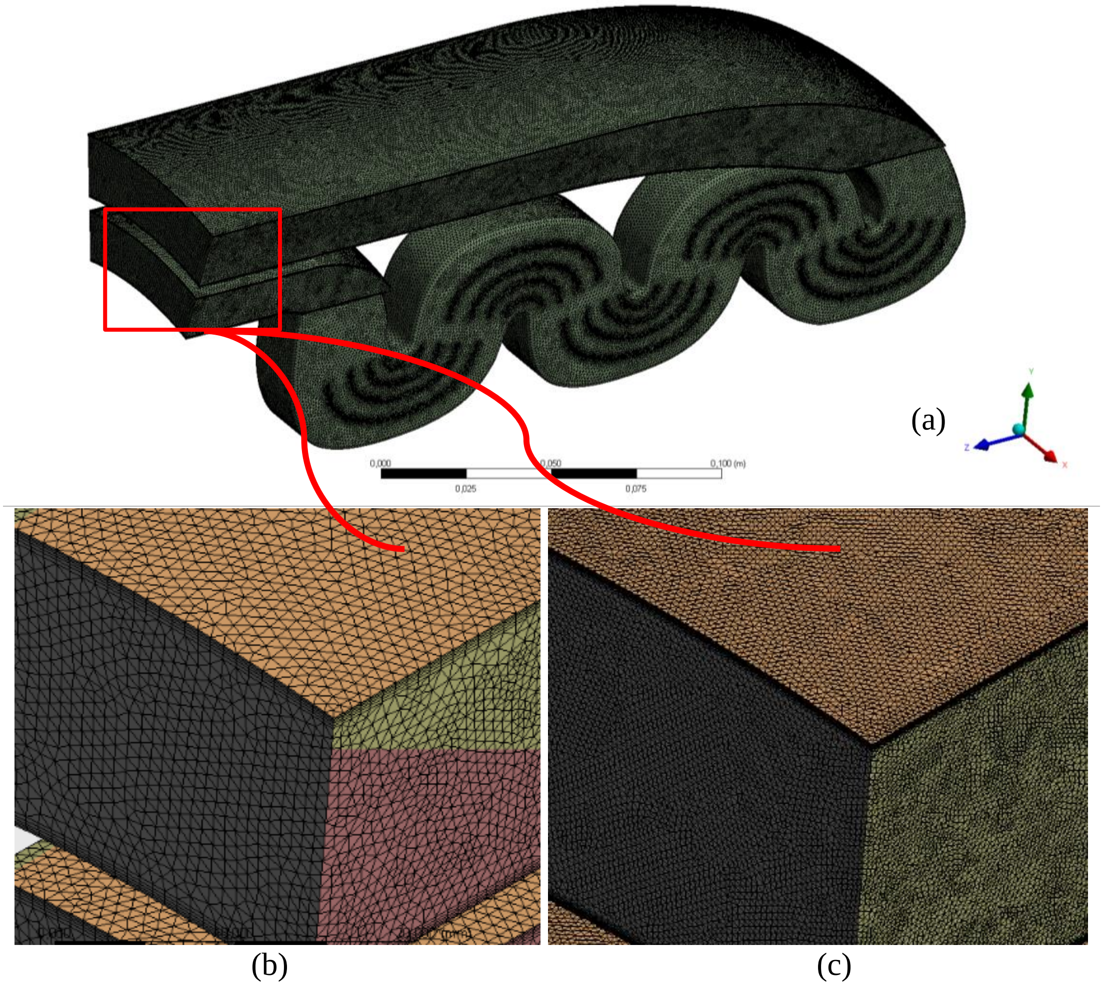

Figure 2.12: (a) Whole mesh structure, (b) fine and (c) coarse mesh in a closer view of the heat exchanger

2.1.4 Validation

Considering Turbulence is a significant topic for Computational Fluid Dynamics (CFD), which is fluid eddy motion characterized by chaotic changes. This chaotic eddy motion has profound effects on many problems such as internal and external flow by causing pressure drop and enhanced heat transfer. For this reason, achieving an accurate turbulent model is important for CFD analyses. In this study, experimental data of heat transfer in a u-bend flow is considered. The experimental set up of Verstraete et al. [13] consists of a centrifugal blower, settling chamber and the test section. This section has a u-bend Plexiglas channel as shown in figure 2.13. This channel is about 2 m long and has a square cross-section. According to reference study, the fluid properties, the bulk velocity, and the hydraulic diameter define the Reynolds number, which is kept at 40,000 for all measurements at the inlet section. On the other hand, Verstraete et al. used steady-state liquid crystals thermography to obtain detailed information on the local heat transfer coefficient.

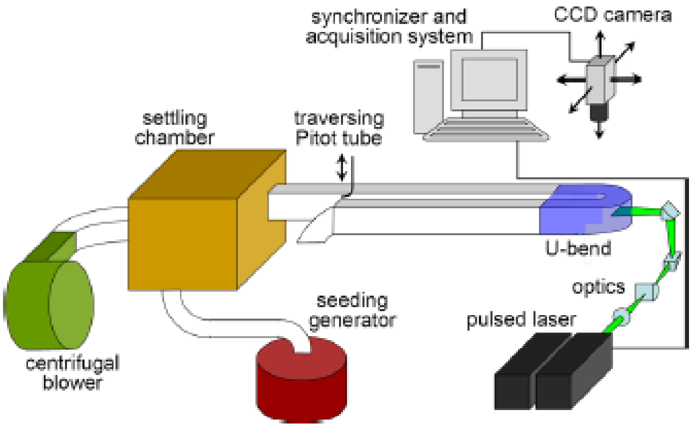

Figure 2.13: Schematic represeation of the experimental set up [13]

Verstraete et al studied the design of a U-bend for serpentine internal cooling channels optimized for minimal pressure loss. In the figure 2.14, the u-bend geometry and dimensions are shown which are used for the experiment. Also, the same geometry and dimensions are studied in this study. A 2.2-kW centrifugal blower discharging into a settling chamber arranges the air flow. Then, fluid flow passes through the test section, which is made of Plexiglas channel. These channels consist of a square cross-section of hydraulic diameter D_h=75 mm and the length is 2 m. The walls are 15mm thick and hermetically sealed. Inlet and outlet location planes are shown in Fig 2.11. The operating conditions are measured in the inlet section by a traversing Pitot probe (diameter 1.5 mm), and a thermocouple located 16 D_h downstream of the settling chamber. At this location, the fluid properties, the bulk velocity, and the hydraulic diameter define the Reynolds number, which is kept at 40,000 for all measurements (the bulk velocity is about 8.8 m/s).

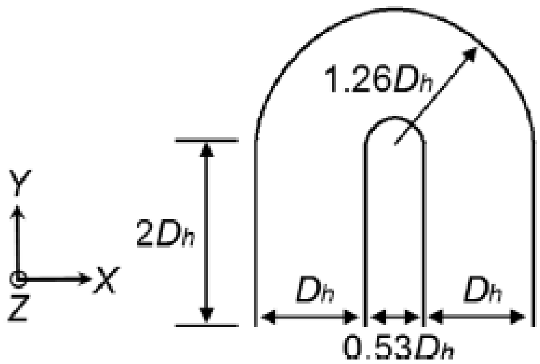

Figure 2.14: U-bend geometry for the standard configuration

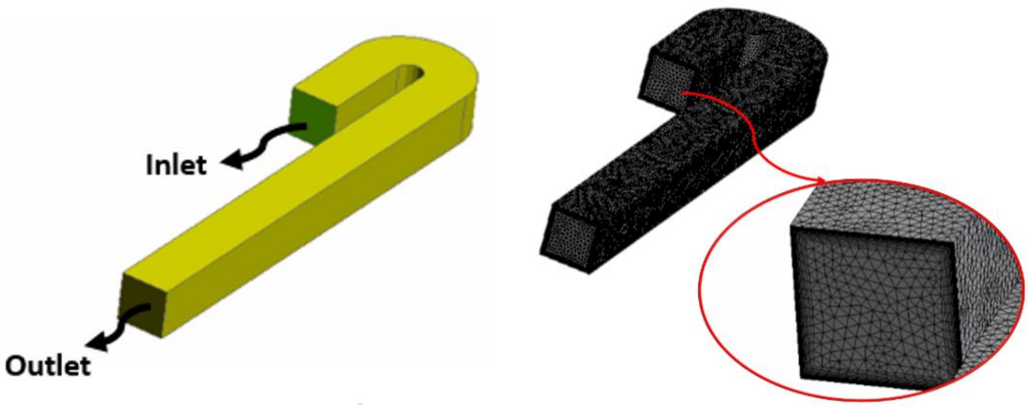

Figure 2.15 The design of the geometry and mesh model in 3D simulation

Studying with an accurate turbulent model is also critical in u-bend flow problems due to the serious effects of the bend geometry types on turbulence. Nevertheless, the streamline curvature and the associated secondary flows essentially affect reproducing in numerical simulations. Two-equation eddy-viscosity models can be helpful for this problem. However, these models can be insufficient to express the streamline curvature effects because of the anisotropy of turbulence. On the other hand, using two-equation model causes low computational cost in industrial applications.

In this study, to match the experimental data, different eddy-viscosity and Full Reynolds-Stress turbulence models are compared such as variants of k epsilon, k-omega and Reynolds Stress model. During this comparison, the experimental design has been modeled in simulation and analyzed with the proper mesh structure. Figure

2.15 shows the designed geometry and mesh model of CFD analysis. The parameter considered during the investigation is the surface Pressure Drop Coefficient and Nusselt Number which is defined as

$$Nu = \frac{hD_h}{k_{air}} \tag{2.1}$$

where k_{air} is the air thermal conductivity and the heat transfer coefficient h is calculated as

$$h = \frac{q - q_{loss}}{T_w - T_b} \tag{2.2}$$

The Nusselt number is normalized by the Dittus–Boelter correlation for a fully developed turbulent flow in a smooth circular tube,

$$Nu_0 = 0.023Re^{0.8}Pr^{0.4} \tag{2.3}$$

The results have been compared regarding the normalized Nusselt number distributions included in the experimental study. Figure 2.16 shows Normalized Nusselt number distributions of experimental study and k-omega with standard wall function k-epsilon realizable with scable wall function CFD results have been compared. However, according to the results, studying turbulence models without wall functions was not sufficient concerning similarity between the experimental and simulation Nusselt number distribution. Consequently, the k-epsilon realizable model has been analyzed with Menter Lechner near-wall treatment. The results of k-epsilon realizable / Menter Lechner have been obtained very close to the normalized Nusselt number distribution of the experiment as shown in figure 2.17.

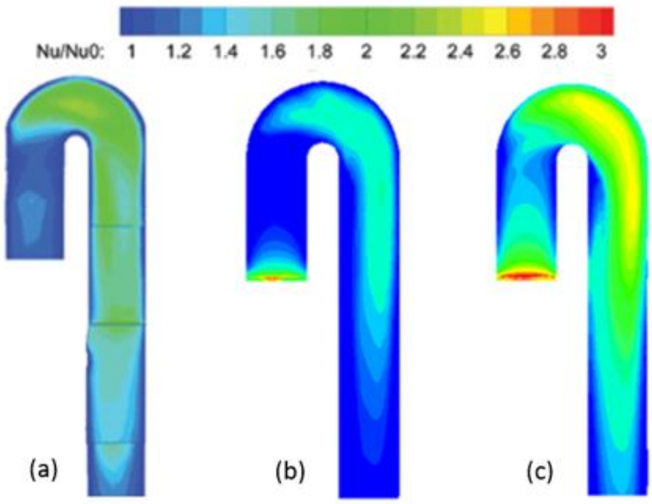

Figure 2.16: Normalized Nusselt number distributions of (a) experimental study, (b) k-omega / standard wall function (c) k-epsilon realizable / scable wall function.

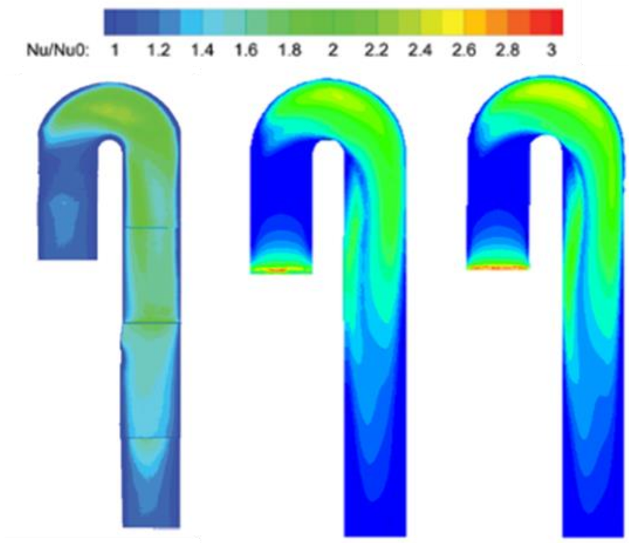

(a) (b) (c)

Figure 2.17: Normalized Nusselt number distributions of (a) experimental study and different mesh configuration: (b) k epsilon realizable Menter Lechner with coarse mesh (c) k epsilon realizable Menter Lechner with fine mesh

In addition, the study of mesh independence on the main subject is also counted in this chapter. The k-epsilon realizable turbulence model using the Menter Lechner wall function has been analyzed by including boundary layer mesh. When the results of the fine and relatively coarse mesh models have been compared, it was observed that the normalized Nusselt number difference was insignificant to be taken into consideration. Therefore, the coarse mesh model can be used in the study.

2.2 Thermodynamic Cycle Analysis based on Component Performance Maps

In this study, after compressor-turbine matching process, a thermodynamic performance calculation code has been developed with using the MATLAB program to accurately compare the values found as a result of the analysis. While comparision, the minimum effectiveness value of the heat exchanger, which provides zero benefit, has been calculated according to the pressure losses. Thus, ratio of current effectiveness calculated according to the analysis results and minimum required effectiveness has been compared.

There are 2 alternatives for the use of components in gas turbine engine studies, using a new compressor and turbine at a certain efficiency and compression ratio, or matching the performance of existing components for working together. In this way, the operating points of the compressor and turbine, whose characteristics are known, are determined at the same rotational speed with various calculations. Calculations are accomplished using compressor and turbine performance graphs in this method. These graphs show the variation of different compression ratios at different rotational speed values according to the standardized mass flow rate. Standardized means values that can be used in all conditions, regardless of the test location of the component. In order to do this, first of all, pressure and temperature values must be standardized.

$$\delta = \frac{P_t}{P_{atm}} , \qquad \theta = \frac{T_t}{T_{atm}} \tag{2.4}$$

Equation 2.4 shows the pressure and temperature constants required to standardize. By finding these values, the std mass flow rate is obtained by equation 2.5.

$$m_{std} = \frac{m\sqrt{(\theta)}}{\delta}, \quad N_{std} = \frac{N}{\sqrt{(\theta)}} \tag{2.5}$$

As equation 2.6 shows, the mass flow of air passing through the compressor is equal to that of leaving the turbine. However, considering the bleed to cool combustion chamber B_C and the addition of fuel f in this equation, the equation becomes 2.7.

$$\dot{m}_C = \dot{m}_T \tag{2.6}$$

$$(1 - B_C)(1 + f)\dot{m}_C = \dot{m}_T \tag{2.7}$$

As mentioned above, standardized mass flow rates are used in performance charts. Nevertheless, turbine curves overlap each other when standard flow rates are taken. This may cause problems in finding the operating points where compressor and turbine works together. Therefore, the standard flow rates are multiplied by the standardized rotational speed to obtain a new corrected mass flow rate as shown in equation 2.8.

$$\frac{\dot{m}_T\sqrt{(\theta_T)}}{\delta_T}\frac{N}{\sqrt{(\theta_T)}} = \frac{\dot{m}_T N}{\delta_T} \tag{2.8}$$

The same correction process is applied to the compressor mass flow rate to create equal conditions.

$$(1 - B_C)(1 + f)\frac{1}{P_T/P_C}\frac{\dot{m}_C N}{\delta_C} = \frac{\dot{m}_T N}{\delta_T} \tag{2.9}$$

This is the first step in the corrected mass flow matching process. The second step is to differentiate the total enthalpy due to power. The dimensionless coefficient $\Delta H_T/N^2$ can be used for the turbine output power which required for working the compressor. The bleed to cool combustion chamber B_C and power for auxiliary elements $P/\dot{m}_C$ not taken into account in this study.

$$\frac{1}{(1 - B_C)(1 + f)}\frac{1}{N^2}\left(\Delta H_C + \frac{P}{\dot{m}_C}\right) = \frac{\Delta H_T}{N^2} \tag{2.10}$$

After matching the compressor and turbine performance maps, as mentioned above, calculating the temperature and pressure of the air at different stations in the brayton cycle is the second step of the thermodynamic analysis section. Since the air is the primary fluid for the application, the following equation represents the ideal gas relation where p identifies pressure, ρ represents density of a fluid and R means that the gas constant with a dimension of J/kgK.

$$p = \rho RT \tag{2.11}$$

and

$$\Delta h = h_2 - h_1 = c_p(T_2 - T_1) \tag{2.12}$$

For ideal gases with constant specific heats, the change in entropy, Δs , for any process can be computed from Tds relation as it is shown that the next equation 2.13

$$\Delta s = s_2 - s_1 = c_p\, ln\frac{T_2}{T_1} - Rln\frac{p_2}{p_1} \tag{2.13}$$

In order to analyse the one-dimensional compressible flows of an ideal gas with constant specific heats, the upper equations are necessary. In this study, the air is assumed as an ideal gas with constant specific heats. Besides these assumptions, in order to obtain the total values isentropic relations are used. The isentropic means that the entropy of a system is constant. The state of s_2 and s_1 equals to each other, then the equation 2.13 becomes:

$$T_1\, p_1^{(1-k)/k} = T_2\, p_2^{(1-k)/k} = T\, p^{(1-k)/k} = constant \tag{2.14}$$

In control volume analysis of fluid dynamics, the enthalpy equation is widely used because it helps to express the internal energy of a fluid and the flow of energy in a single term. In the high-speed flows, such as jet engines, the potential energy of fluid can be neglected but the kinetic energy is not. In these circumstances, the enthalpy and the kinetic energy of the fluid into a single term called stagnation (or total) enthalpy h_0, defined by per unit mass as,

$$h_0 = h + \frac{V^2}{2} \qquad kj/kg \tag{2.15}$$

Throughout this chapter the ordinary enthalpy h is referred to as the static enthalpy, whenever necessary, to distinguish it from the stagnation enthalpy. For the steady flow of a fluid through a duct such as a nozzle, diffuser, or some other flow passage where the flow takes place adiabatically and with no shaft or electrical work with the assumption as the no elevation change is observed and the energy is balanced for single-stream steady flow system can be defined by the following expression eq. 2.16.

$$h_1 + \frac{V_1^2}{2} = h_2 + \frac{V_2^2}{2} = h_{01} = h_{02} \tag{2.16}$$

The stagnation state is detected as the isentropic stagnation process when the stagnation operation is reversible as well as adiabatic (i.e., isentropic) and the entropy of a fluid remains constant during an isentropic stagnation process. In this study, the fluid is approximated as an ideal gas with constant specific heats and the equations become

$$T_0 = T + \frac{V^2}{2c_p} \tag{2.17}$$

Where T_0 is named as the stagnation temperature and $V^2/2c_p$ term represents the dynamic temperature that provides the temperature rise during a process. Moreover, at isentropically rest pressure of the fluid is called as the stagnation pressure P_0. For ideal gases with specific constant heats, P_0 and static pressure P have a relation,

$$\frac{P_0}{P} = \left(\frac{T_0}{T}\right)^{\frac{k}{k-1}} \tag{2.18}$$

and from the ideal gas equation static density and total density can be obtain by using the following expressions

$$\frac{\rho_0}{\rho} = \left(\frac{T_0}{T}\right)^{\frac{1}{k-1}} \tag{2.19}$$

The energy balance of a single flow-through flow device represents 1 and 2, where 1 represents the inlet and 2 symbolizes the outlet stations:

$$q_{in} - q_{out} + w_{in} - w_{out} = c_p(T_{02} - T_{01}) + g(z_2 - z_1) \qquad (2.20)$$

with T_{02} and T_{01} are the stagnation temperatures.

In the compressible flow applications, the speed of sound, c and Mach number, M are exceptional parameters. For an ideal gas where the speed of sound is only a function of temperature. The other parameter that is important to determination of the compressible flow operations is Mach Number M which is identified by Australian physicist Ernst Mach in 1838. Mach number is a ratio of the actual velocity of the fluid or fluid particle which moves in a fluid medium to speed of sound for the same environment:

$$c = \sqrt{kRT} \qquad (2.21)$$

$$M = \frac{V}{c} \qquad (2.22)$$

Flow regimes are often expressed in terms of Mach numbers. The flow regime is sonic for $M = 1$, supersonic for $M > 1$ and subsonic for $M < 1$, besides when $M \gg 1$, the flow is hypersonic and $M \cong 1$, the flow becomes transonic.

First, we should find energy balance equation of this system. The changes in kinetic and potential energies are neglected, the energy balance for a steady-flow process can be expressed as

$$(q_{in} - q_{out}) + (w_{in} - w_{out}) = h_{out} - h_{in} \qquad (2.23)$$

Therefore, heat transfers to and from the working fluid are

$$q_{in} = h_3 - h_2 = c_p(T_3 - T_2) \tag{2.24}$$

and

$$q_{out} = h_4 - h_1 = c_p(T_4 - T_1) \tag{2.25}$$

Then the thermal efficiency of the ideal Brayton cycle under the cold-air standard assumptions becomes

$$\eta_{Brayton} = \frac{W_{net}}{q_{in}} = 1 - \frac{q_{out}}{q_{in}} = 1 - \frac{c_p(T_4 - T_1)}{c_p(T_3 - T_2)} \tag{2.26}$$

The actual gas-turbine cycle is different from the ideal Brayton cycle since there are irreversibilities. Hence, in an actual gas-turbine cycle, the compressor consumes more work and the turbine produces less work than that of the ideal Brayton cycle. The irreversibilities in an actual compressor and an actual turbine can be considered by using the adiabatic efficiencies of the compressor and turbine. The deviation of an actual compressor and turbine behavior from the idealized isentropic behavior can be accurately accounted for by utilizing the isentropic efficiencies of the turbine and compressor as

$$\eta_{comp.} = \frac{W_s}{W_a} = \frac{h_{2s} - h_1}{h_{2a} - h_1} \tag{2.27}$$

$$\eta_{turb.} = \frac{W_a}{W_s} = \frac{h_3 - h_{4a}}{h_3 - h_{4s}} \tag{2.28}$$

Thrust is a reaction force that is produced by accelerating a gas. This force is based on Newton's third law of motion. Thrust formula is,

$$F_{thrust} = \dot{m}_9 V_9 - \dot{m}_0 V_0 + (P_9 - P_0) A_9 \tag{2.29}$$

For airbreathing engines, the only thrust force is not sufficient as a parameter for comparison in different circumstances. Therefore, the ratio of fuel mass flow rate per unit thrust force is meaningful for these problems.

$$TSFC = \frac{\dot{m}_f}{F_{thrust}} \tag{2.30}$$

The minimum required effectiveness is a crucial point due to changing with pressure loss. To put it another way, a new min effectiveness value must be calculated for each new analysis. The thermodynamic performance analysis in the MATLAB program, which is explained in table 2.1 as a flow chart, is aimed to calculate this parameter by using the above equations. Basically, Appendix A shows software, the SFC value of the cycle without the recuperator has been considered as zero benefits, and the new minimum required effectiveness has been investigated by taking into account the new pressure losses using the iteration method. While doing this, new matched operation points should be obtained in each iteration as compressor turbine matching operation points also change with new iterative values.

Table 2.1: The flow chart of thermodynamic cycle analysis

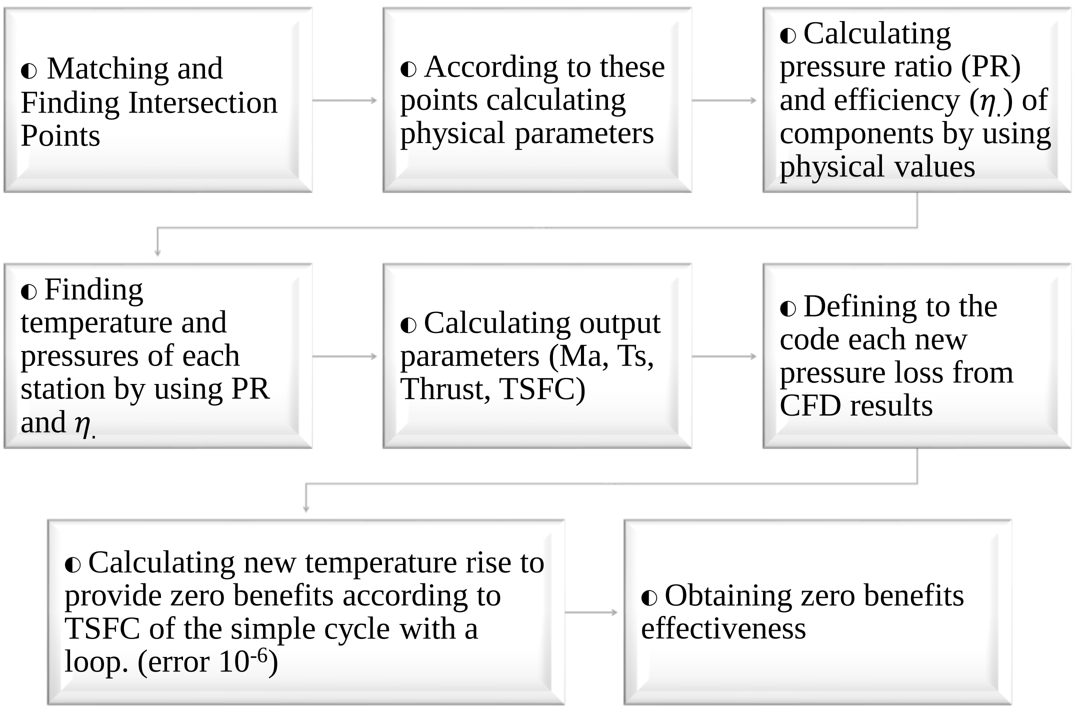

After estimating the initial temperature rise and fuel flow rate, the code loop starts with matching. Compressor turbine performance maps provided from different studies have been integrated into the code and by using pressure ratios from the map and considering other losses (i.e combustion chamber), compressor inlet-outlet pressures have been calculated. In addition, after calculating δ and θ of the compressor and turbine using equation 2.4, the corrected mass flow rates shown in equation 2.9 have been accomplished. Due to the corrected enthalpy differences calculated with equation 2.10, the physical values at that point have been found again after obtaining the intersecting operating points in the compressor and turbine performance maps.

Eventually, values such as Mach number, jet velocity, thrust, SFC have been calculated with thermodynamic cycle formulas as mentioned above. In the loop which is developed with 10^{-6} errors, the required min effectiveness has been obtained with the constant old SFC value (without the recuperator) and the new temperature, etc. values.

Chapter 3

The Efficient Concept Suitable for Land Micro Gas Turbines

3.1 CFD Results of Recuperator and Its Thermodynamic Effect on The Engine

In this chapter, the comparative results of the 3D models analyzed using the methods mentioned above have been shown. Different temperature rises have been obtained in the CFD analyzes of these models due to each of them has a different number of leaves. Changes in the amount of heat transfer make the difference in effectiveness values inevitable. On the other hand, pressure losses owing to different tube thicknesses caused by leaf differences are the reason for the change in the minimum required effectiveness values for each model. As a result, the effectiveness/threshold effectiveness ratio has been considered during these comparisons. Figure 3.1 shows the effectiveness graph based on the different number of leaves. In the first case, although all models have an effectiveness value higher than zero benefits in figure 3.1a, the highest effectiveness ratio has been reached in model 16 leaves. Apart from that, in the second case, the results of the model 20 leaves represent the critical point on the graph as shown in figure 3.1b. While models 12 and 16 leaves are accomplished, the effectiveness ratio is less than one in models which have a higher number of leaves than 20. In summary, the comparative results show that the radial tube is more efficient than the curved tube in the case of multiple u-bend bodies.

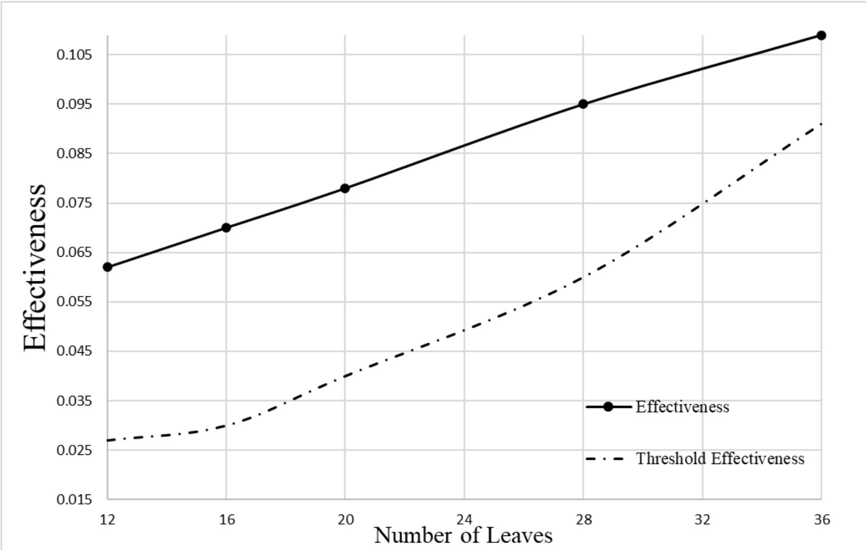

(a)

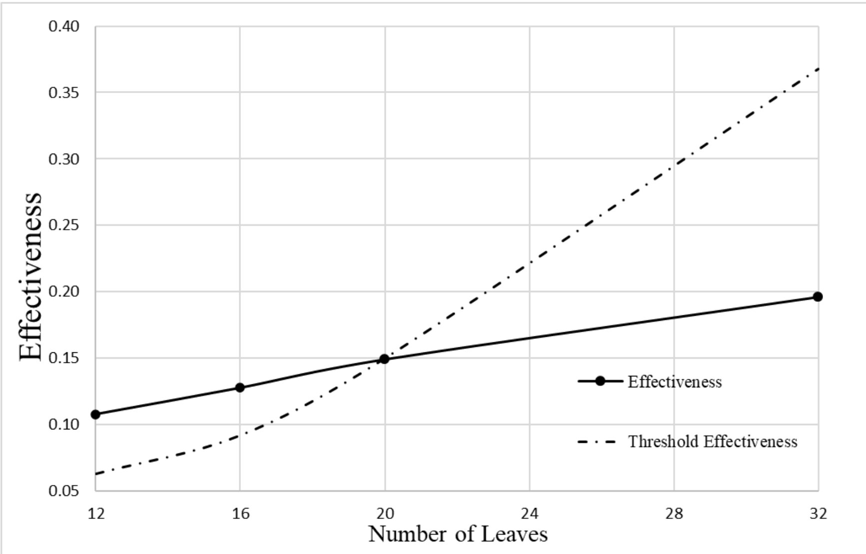

(b)

Figure 3.1: Comparison graph of the different number of leaves results: Multiple u-bend body, (a) Case 1, (b) Case 2

In addition to the tube studies, two different manifold designs have been compared. The effectiveness ratio of the first model, in which the fluid from the tube to the components is collected in a single pipe, is higher than the second model. In the second manifold design, which depends on the number of leaves, higher pressure losses associated with more surfaces cause the threshold effectiveness value almost twice. The ratio of the multi-manifold model is lower considering these results where the temperature rise remains constant.

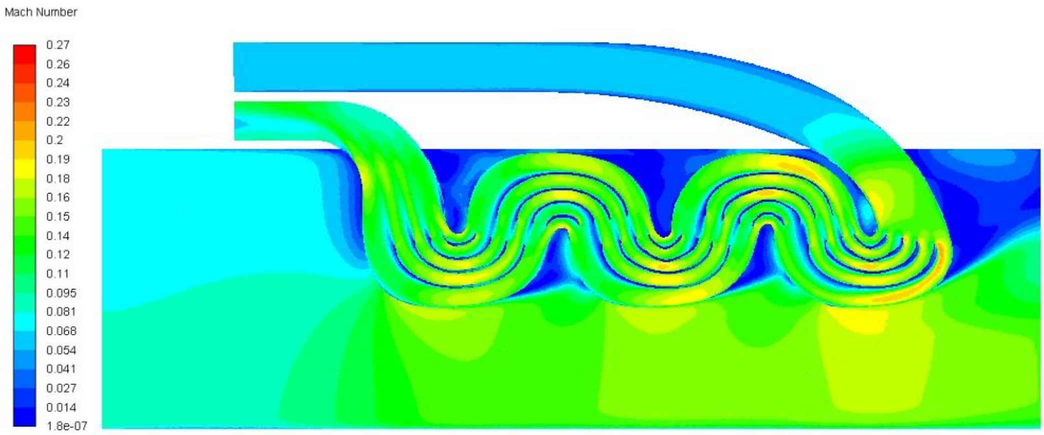

Figure 3.2: The contour of Mach number from CFD results of land type

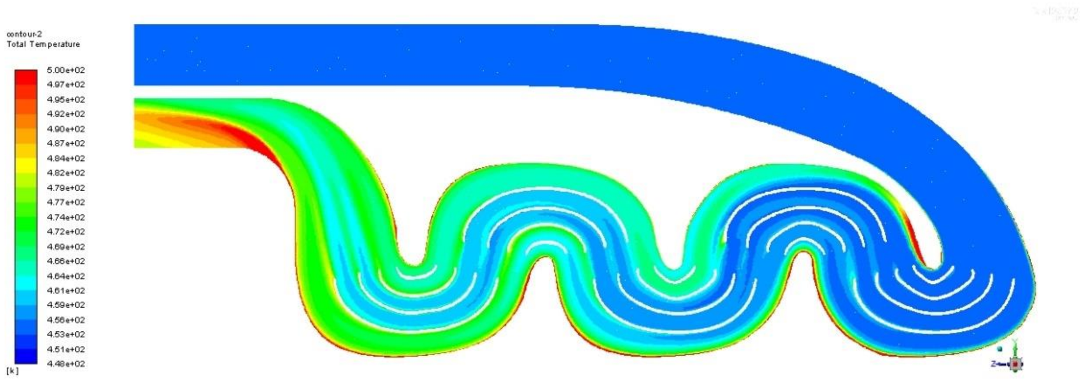

Figure 3.3: The contour of temperature distrubition from CFD results of land type

In addition, the Mach number and temperature distribution contours of the optimum model have been shown in figure 3.2 and figure 3.3. These results have been obtained from the isosurface of a leaf in angular coordinates. Although figure 3.2 consists of the combination of hot (rectangular face) and cold bodies, figure 3.3 shows the only cold body. Because there are high-temperature differences between bodies and it causes a meaningless legend in the contour.

Table 3.1: The thermodynamic performance parameters of recuperator for land turbojet type

	Simple Cycle	Recuperated Cycle	Percent Change %
Fuel Mass Flow Rate ($\dot{m}_f$)	0.019132 kg/s	0.018217 kg/s	4.78 ⇩
Thrust (F_{thrust})	707.33 N	691.06 N	2.30 ⬇
TSFC	27.048 g/s.kN	26.361 g/s.kN	2.54 ⇩
Specific Thrust	470.52 Ns/kg	459.57 Ns/kg	2.33 ⬇

According to CFD results of efficient concepts, two different cases have been investigated as turbojet which corresponds to thrust, and turbofan which corresponds to thermal efficiency with an additional turbine. Table 3.1 shows the thermodynamic parameter results of turbojet type. According to these results, fuel consumption in the recuperator engine has decreased by approximately 5 percent compared to the simple engine whereby the effective heat exchanger. Nevertheless, pressure losses due to the added heat exchanger caused a 2.3 percent decrease in thrust. Although it seems the losses in thrust have a negative effect, a 2.5 percent reduction in thrust-specific fuel consumption (TSFC) is beneficial for the engine. Lastly, the specific thrust, which shows the amount of thrust generated per mass flow rate, has decreased by 2.33 percent due to pressure losses. However, the land turbine concept is unaffected from the thrust and therefore TSFC is more important, whereby a larger specific thrust means a less compact engine.

Table 3.2: The thermodynamic performance parameters of recuperator for land turbofan type

	Simple Cycle	Recuperated Cycle	Percent Change %
Fuel Mass Flow Rate ($\dot{m}_f$)	0.019687 kg/s	0.018774 kg/s	4.64 ⇩
Power	166.02 N	158.58 W	4.48 ⬇
Thermal Efficiency	20.08%	20.11%	1.49 ⇧

In the second case with an additional turbine to the engine, fuel consumption, power required for the second turbine and thermal efficiency of the engine have been investigated. Though power has decreased 4.48% compared to the simple engine, fuel consumption has decreased 4.64%. Moreover, when thermal efficiencies have been compared, there exists a 1.49% improvement. However, as shown in the tables, the improvements of the turbofan engine aren't as favorable as turbojet. Hence, using this recuperator model in turbojet engines with larger diameters is more logical than turbofan.

3.1.1 Mesh Independency

For CFD analysis, the mesh model is important for the accuracy of the results and time-saving. Therefore, in this thesis, a total of 6 different mesh models, 3 medium and 3 fine have been analyzed. The results have been evaluated separately in terms of two main parameters, pressure and temperature, as shown in figures 3.4 and 3.5. Comparisons have been evaluated against the finest mesh model, where the results have been almost unchanged. According to the graphs, the initial point of stabilization is model 4 (finer 1). However, when compared with the finest mesh model, it has been obtained that the difference between model 3 (medium 3) and model 4 (finer 1) was almost equal to the finest mesh model. Moreover, the temperature difference of medium 3 is less than finer 1. Thus, the medium 3 mesh model has been preferred instead of finer 1.

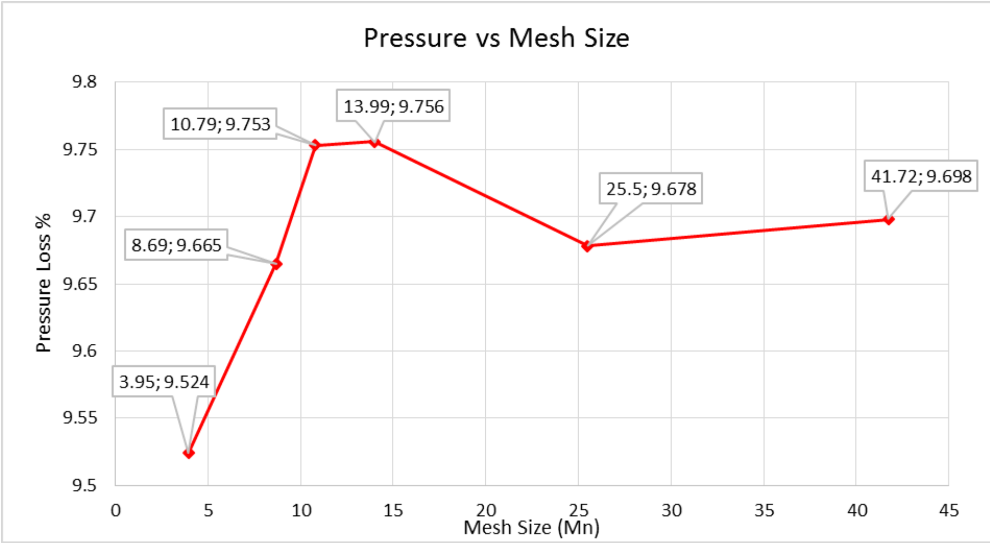

Figure 3.4: Comparison graph of the different mesh size with respect to pressure drop

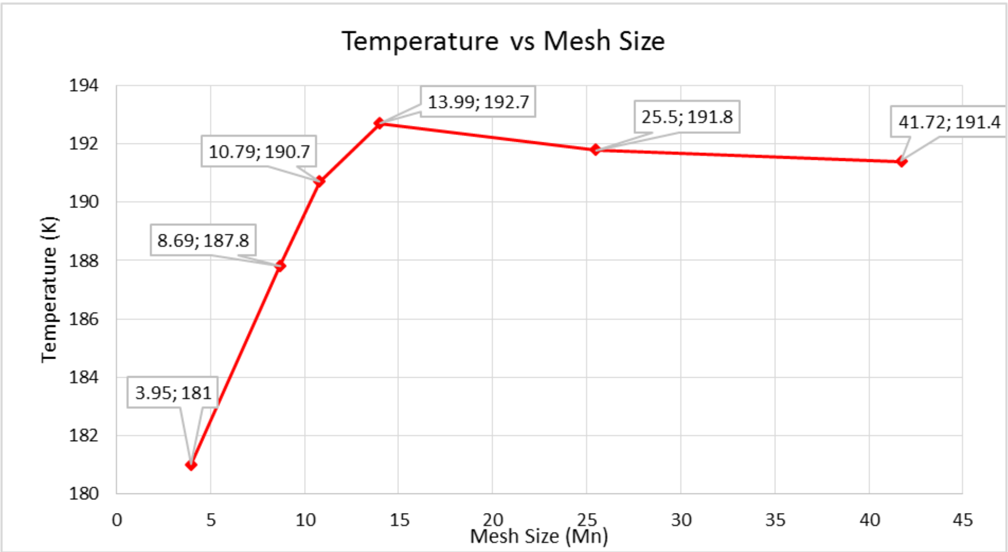

Figure 3.5: Comparison graph of the different mesh size with respect to temperature

Chapter 4

The More Compact Concept Suitable for Aero Micro Gas Turbines

Micro gas turbines used in aviation should be more compact than those used on the ground due to the space limitations, was mentioned. In this circumstance, high pressure losses do not allow multiple u-bend tubes. The single u-bend recuperator type for the aero-engine has been evaluated according to the cases represented by three different cross-sectional areas.

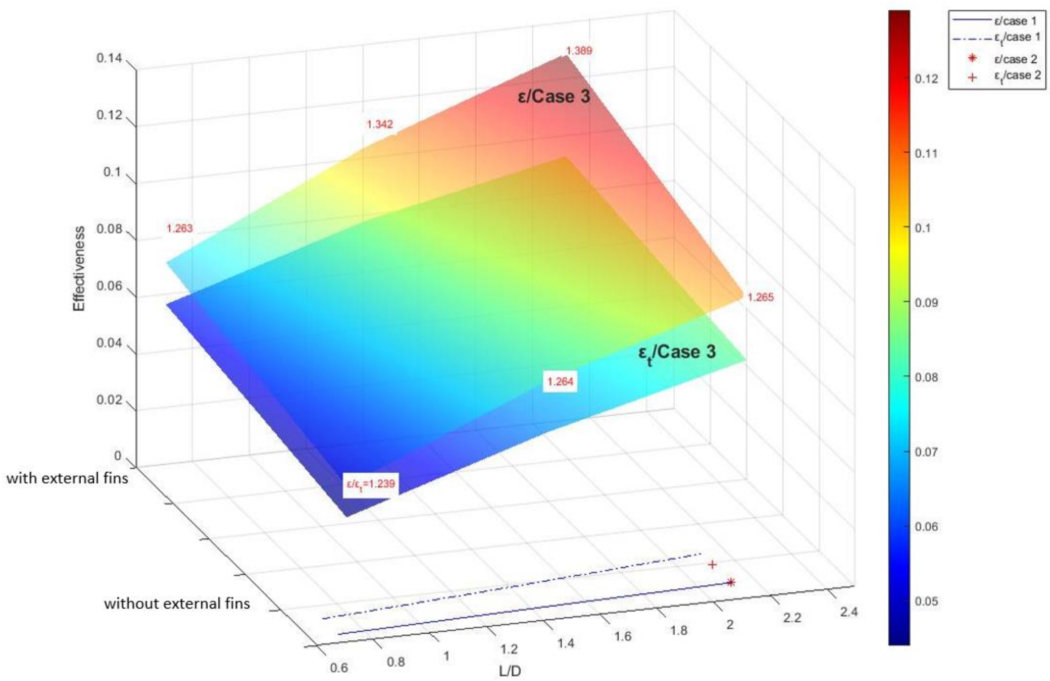

Figure 4.1: The results of single u-bend heat exchanger models for micro gas turbine in different cases

In the comprehensive result graph, as shown in Figure 4.1, unlike the floor type, the effectiveness depends on the ratio of the tube length (L) to the motor diameter (D). According to the analysis results of the first case, the threshold effectiveness is higher than the current value for all L/D ratios. Therefore, the effectiveness ratio is less than one. Furthermore, case 2 was analyzed with only one L/D ratio to avoid wasting time. According to this result, the current effectiveness value is lower than the threshold, just like the first case. Besides, the latest model has been successful in different L/D values with its high effectiveness value and ratio. The effectiveness has been increased by adding outer fins to the geometry which has been designed with only inner fins before. With the expanding surface area required for heat transfer, the finned and high L/D ratio model has been obtained as the most efficient.

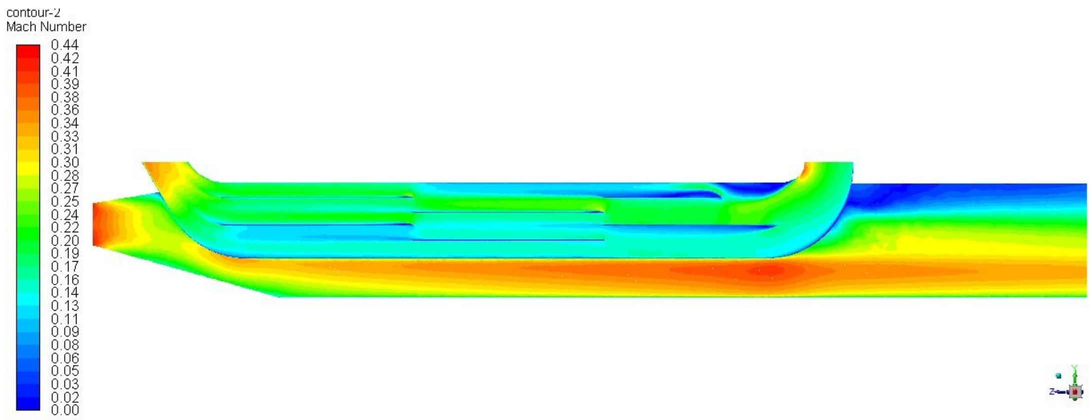

Figure 4.2: The contour of Mach number from CFD results of aero type

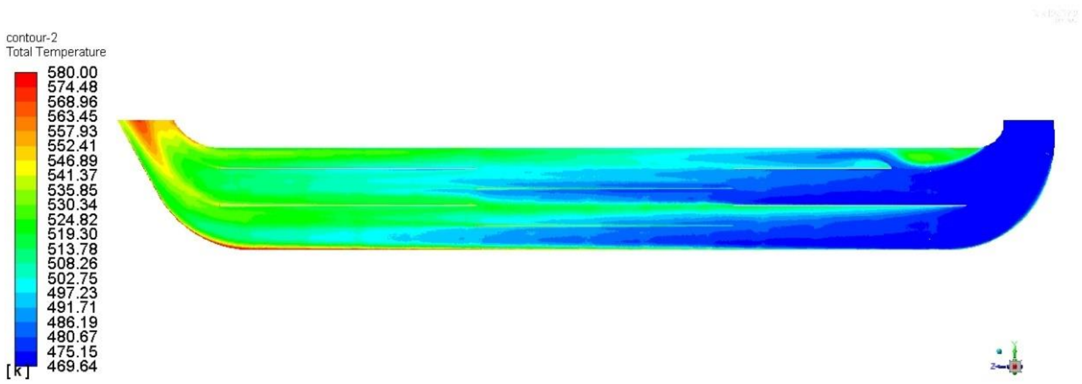

Figure 4.3: The contour of temperature distrubition from CFD results of aero type

Considering to the latest developments, the effectiveness of the heat exchanger reached 14.5%, while the effectiveness ratio increased to 1.58. Thermodynamic analyzes of this model, which is the most effective, have been performed via MATLAB. Also, the Mach number and temperature distribution contours of this model have been shown in figure 4.2 and figure 4.3. These CFD results have been obtained from the isosurface of a leaf in angular coordinates like land type.

On the other hand, the compressor and turbine performance maps of the matching study in the thermodynamic analysis done according to the CFD results have been obtained as shown in figure 4.4 and figure 4.5. As mentioned above, these maps include the variation of the pressure ratio with respect to the corrected mass flow rate and different lines represent the different rotational speeds. In addition, the graph of the corrected enthalpy, which is reached by thermodynamic cycle calculations, constitutes the last step of the matching study. For this reason, intersection points have been obtained when the enthalpy maps of the compressor and turbine have been matched. Hence, these are the operating points and are indicated by the red stars in figure 4.6.

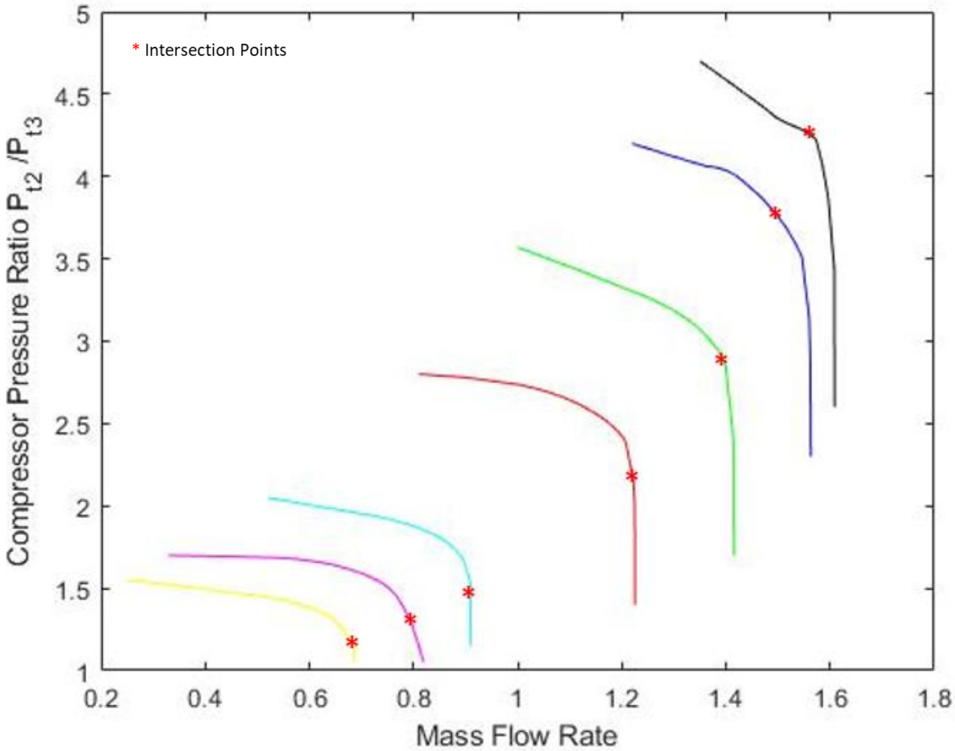

Figure 4.4: The performance map of the compressor

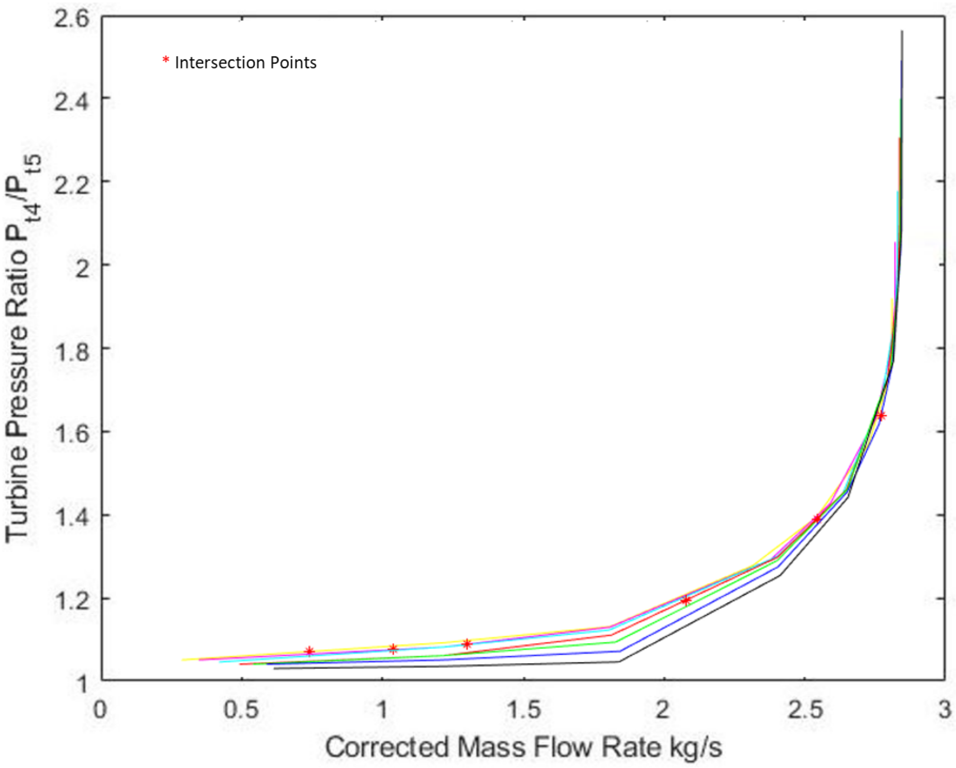

Figure 4.5: The performance map of the turbine

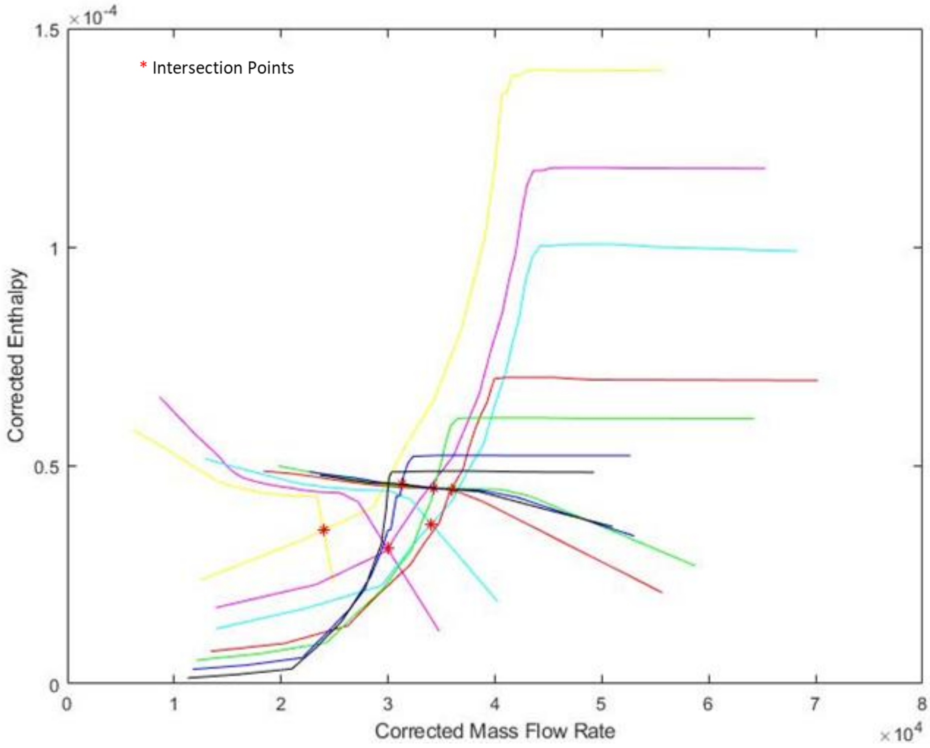

Figure 4.6: Matching of the performance maps

Table 4.1 shows the thermodynamic parameter results of the efficient model for aero engines. As in the recuperator model used for the Land type engine, there exits some loss in thrust in favor of a fuel saving of nearly 10%. As a result, the TSFC of the recuperated engine is approximately 5% lower than the simple cycle, which means less fuel consumption for the same thrust. However, this reduces compactness (more diameter and sucked air) of the engine, as evidenced by the 5% smaller specific thrust.

Table 4.1: The thermodynamic performance parameters of recuperator for aero type

	Simple Cycle	Recuperated Cycle	Percent Change %
Fuel Mass Flow Rate ($\dot{m}_f$)	0.019132 kg/s	0.017226 kg/s	9.96
Thrust (F_{thrust})	707.33 N	669.12 N	5.40
TSFC	27.048 g/s.kN	25.745 g/s.kN	4.82
Specific Thrust	470.52 Ns/kg	446.53 Ns/kg	5.10

Chapter 5

Conclusions

Especially commercial and military aviation, electricity generation are some of the application areas of gas turbine engine and it has an important role for the "clean air" studies that are being tried to be implemented today. In the studies with that purpose, heat exchangers are one of the fundamental subjects which are at the exit of the turbine and provide fuel-saving by preheating the air coming out of the compressor to the combustion chamber. Also, in this thesis, a heat exchanger design optimization has been studied for land and aero type micro gas turbine engines with a different geometric design from literature studies.

Balancing power generation in industrial uses, thrust generation in aviation, and the fuel consumption required for them is the target of the study. For this reason, the fact that the designed heat exchanger causes power or thrust loss during fuel saving is a compelling factor. In this regard, minimizing pressure losses in order to prevent power loss and maximizing the temperature rise for fuel-saving are two objectives of the study. How effective the heat exchanger is to parameterize the temperature rise is discussed in this study. Additionally, since the field for design is more constraint in aviation than in industrial uses, a more compact model has been designed for air motors. While comparing the tubes called leaves in different numbers, cross-section areas, and lengths, the effective model with the least pressure loss has been investigated. Since the models with the highest effectiveness ratio are optimum, the number of 16 leaves model has been found to be beneficial for the industrial land motor. Moreover, it has been obtained that the second case, whose cross-sectional area is not radial, is effective only in numbers 20 and below. When the results of 16 leaves are evaluated which has been agreed on as the most optimum model for the land micro gas turbine engine, the fuel mass flow rate decreased by 4.78% compared to the simple cycle without a recuperator. Nevertheless, 2.30% less thrust has been evaluated as a result of pressure losses on the cold and hot sides of the heat exchanger. However, it should be noted that the thrust-specific fuel consumption, which is the deciding factor for the effective model, positively decreased by 2.54%. Apart from that, mesh independence has been studied to ensure accuracy in CFD analysis of the land type engine. In the study performed with 6 different mesh numbers in total, the third medium-mesh model is stable, has a minimum error, and does not waste time. In addition to mesh, turbulence model validation has been performed with an experimental study to specify the accurate analysis method. As a result of the comparisons made according to the Nusselt number distribution, it was obtained that the k epsilon realizable Menter Lechner turbulence model had the closest results.

In this thesis, different from the land model, a heat exchanger study has been investigated for the aero-engine type. Since the biggest difference is the limitation of area, it is aimed that to design the most effective heat exchanger by occupying the least area. However, it is substantial not to increase the pressure loss with a complicated structure. Thus, a single u-turn has been preferred instead of multiple u-turns used in the design of the land type. 3-dimensional CFD analyzes have been done by changing parameters such as cross-sectional area and length, and outer fins have been added to increase the surface area in the optimum model. According to CFD results, a compact model with an effective ratio of 1.58 and effectiveness of 14.5% has been reached. Then, the effects on the engine have been discussed with thermodynamic cycle analysis. While it achieves success with a 9.96% decrease in fuel saving, the thrust loss is only in the 5.40% band. Thus, the recuperator aero-engine has 4.82% less TSFC.

In conclusion, these two designs studied for land and aero type micro gas turbines exceeded the zero-benefit requirement and achieved success with less thrust loss than the amount of fuel savings. Since the recuperator design will be adapted to a prebuilt micro gas turbine engine, the dimensions are limited. Therefore, the effectiveness value of McDonald's models [10] in the previous studies, which is 80-90%, could not be reached. The 15% effective recuperator, designed for the engine with turbine hub diameter 80 mm and shroud diameter 140 mm, can be improved by using different technics such as increasing the diameter, changing material or design of the engine, etc.

References

[1] Çengel Y, Boles M. Thermodynamics: An Engineering Approach, 5th ed. McGraw-Hill; 2001.

[2] Jansohn P. Overview of Gas Turbine Types and Applications. Ed.: Jansohn P. Modern Gas Turbine Systems. Woodhead Publishing; 2013. 21-41.

[3] Boyce M. Gas Turbine Engineering Handbook, 2th ed. Gulf Professional Publishing; 2002.

[4] GE Gas Power. The 7E.03 Gas Turbine [Internet]. New York; 2021 [25.10.2021]. https://www.ge.com/gas-power/products/gas-turbines/7e.

[5] Capstone Green Energy. C65 Gas Turbine [Internet]. Los Angeles; 2021 [25.10.2021]. https://www.capstonegreenenergy.com/products/energyconversionproducts/capstone-microturbines/c65

[6] MOM A. Introduction to gas turbines. Ed.: Jansohn P. Modern Gas Turbine Systems. Woodhead Publishing; 2013. 3-20.

[7] Soares C. Gas Turbines: A Handbook of Air, Land and Sea Applications, 2th ed. Butterworth-Heinemann; 2014.

[8] Foerster S, Kleeman M. Compact Metallic and Ceramic Recuperators for Gas Turbines. ASME 1978; Paper No. 78-GT-62.

[9] McDonald C. Low-Cost Compact Primary Surface Recuperator Concept for Microturbines. Appl. Therm. Eng 2000; 471-497.

[10] McDonald C. Recuperator Considerations for Future High Efficiency Microturbines. Appl. Therm. Eng. 2002; 1453-1487.

[11] Antoine H, Prieels L. The ACTE Spiral Recuperator for Gas Turbine Engines. ASME 2002; Paper No. GT2002-30405.

[12] Treece B, Vessa P, McKeirnan R. Microturbine Recuperator Manufacturing and Operating Experience. ASME 2002; Paper No. GT2002-30404.

[13] Verstraete T, Coletti F, Bulle J, Van der Wielen T, Arts T. Optimization of a U-Bend for Minimal Pressure Loss in Internal Cooling Channels: Part II—Experimental Validation. Journal of Turbomachinery 2013; 135(5)

Appendices

Appendix A

Thermodynamic Cycle Analysis Code based on Component Performance Maps on MATLAB

```
%% Recuperator Thermodynamics Performance Calculator with Matching

TR=24; %Initial value for temperature rise

initial_f= [0.0163; 0.0161; 0.0156; 0.0143; 0.0121; 0.0121; 0.0122]; %Initial Guess

for j=1:100

% Matching

mfr_2(:,1)=[0.25 0.3 0.383 0.4045 0.426 0.4475 0.469 0.4905 0.512 0.5335 0.555 0.5765 0.598 0.6195 0.641 0.6625 0.684 0.685 0.6855];

mfr_2(:,2)=[0.33 0.45 0.542 0.5593 0.5766 0.5939 0.6111 0.6284 0.6457 0.663 0.6803 0.6976 0.7149 0.7321 0.7494 0.7667 0.784 0.795 0.82];

mfr_2(:,3)=[0.52 0.61 0.704 0.7187 0.7333 0.748 0.7627 0.7774 0.792 0.8067 0.8214 0.836 0.8507 0.8654 0.8801 0.8947 0.9094 0.9098 0.91];

mfr_2(:,4)=[0.81 0.9 1 1.0159 1.0317 1.0476 1.0634 1.0793 1.0951 1.111 1.1269 1.1427 1.1586 1.1744 1.1903 1.2061 1.222 1.225 1.2255];

mfr_2(:,5)=[1 1.11 1.22 1.2338 1.2476 1.2614 1.2751 1.2889 1.3027 1.3165 1.3303 1.3441 1.3579 1.3716 1.3854 1.3992 1.413 1.415 1.4156];
```

mfr_2(:,6)=[1.22 1.29 1.362 1.3761 1.3903 1.4044 1.4186 1.4327 1.4469 1.461 1.4751 1.4893 1.5034 1.5176 1.5317 1.5459 1.56 1.562 1.563];

mfr_2(:,7)=[1.35 1.39 1.446 1.4576 1.4692 1.4807 1.4923 1.5039 1.5155 1.5271 1.5386 1.5502 1.5618 1.5734 1.5849 1.5965 1.6081 1.6085 1.609];

CPR(:,1)=[1.55 1.533 1.501 1.4925 1.484 1.4754 1.4667 1.458 1.4498 1.4395 1.4244 1.4065 1.3862 1.3604 1.3253 1.2627 1.157 1.12 1.05];

CPR(:,2)=[1.7 1.693 1.685 1.6818 1.6766 1.6699 1.6622 1.6535 1.6418 1.6275 1.6117 1.5938 1.5722 1.5453 1.5116 1.4567 1.366 1.3 1.05];

CPR(:,3)=[2.05 2 1.95 1.9431 1.9343 1.9238 1.912 1.8992 1.8854 1.87 1.8523 1.8313 1.8065 1.7763 1.736 1.6803 1.536 1.44 1.15];

CPR(:,4)=[2.8 2.78 2.737 2.7266 2.7146 2.7014 2.6867 2.6697 2.6499 2.6273 2.6018 2.5733 2.5421 2.5056 2.4606 2.4021 2.169 2 1.4];

CPR(:,5)=[3.57 3.44 3.303 3.287 3.2687 3.2491 3.2282 3.2055 3.1806 3.1532 3.1232 3.0891 3.0475 2.9962 2.9454 2.8519 2.458 2.3 1.7];

CPR(:,6)=[4.2 4.13 4.062 4.0578 4.0469 4.0315 4.0073 3.9717 3.9334 3.8921 3.8478 3.7975 3.7428 3.6795 3.6038 3.5133 3.143 2.9 2.3];

CPR(:,7)=[4.7 4.61 4.481 4.4549 4.4275 4.3991 4.3681 4.3438 4.3256 4.3101 4.2947 4.277 4.2543 4.2245 4.0775 3.8748 3.44 3 2.6];

eff_co(:,1)=[0.753 0.755 0.76 0.7627 0.7653 0.7679 0.7704 0.773 0.7759 0.7764 0.7624 0.7433 0.717 0.6806 0.6293 0.5215 0.325 0.25 0.2];

eff_co(:,2)=[0.6 0.68 0.748 0.7672 0.7816 0.7911 0.7956 0.7948 0.789 0.7811 0.7707 0.7563 0.737 0.7118 0.6799 0.6212 0.513 0.45 0.28];

eff_co(:,3)=[0.814 0.812 0.809 0.8085 0.8072 0.8051 0.8024 0.7993 0.7953 0.7885 0.7789 0.7667 0.7523 0.733 0.7041 0.6627 0.544 0.48 0.4];

eff_co(:,4)=[0.8302 0.8302 0.83 0.8298 0.8291 0.828 0.8258 0.8229 0.8193 0.8146 0.8087 0.8018 0.7933 0.7822 0.768 0.7484 0.654 0.62 0.57];

eff_co(:,5)=[0.843 0.838 0.829 0.8277 0.826 0.8241 0.8218 0.8192 0.8161 0.8124 0.8079 0.8017 0.7935 0.7832 0.7715 0.7474 0.631 0.6 0.58];

eff_co(:,6)=[0.816 0.815 0.8127 0.813 0.8131 0.8131 0.8118 0.8091 0.807 0.8039 0.7981 0.7916 0.7853 0.7779 0.7684 0.7553 0.683 0.65 0.62];

eff_co(:,7)=[0.815 0.81 0.804 0.8014 0.7992 0.7972 0.7957 0.7939 0.7917 0.7893 0.7867 0.7838 0.7808 0.7777 0.7603 0.7361 0.673 0.64 0.61];

mfr_4(:,1)=[0.515 0.9 1.144787914 1.249895522 1.355003129 1.448637812 1.524892101 1.551583098 1.558621015 1.55959564 1.559642268 1.559687779 1.559687823 1.559640704 1.559687919 1.559680129 1.559665021 1.559666 1.559667];

mfr_4(:,2)=[0.54 0.9 1.144928396 1.263401665 1.381874934 1.468814497 1.502153586 1.535492675 1.547121297 1.55874992 1.563926848 1.564406152 1.564420985 1.564420993 1.564420818 1.564420739 1.564419875 1.5644195 1.5643];

mfr_4(:,3)=[0.57 0.9 1.143745901 1.267165858 1.390585816 1.438692981 1.486800147 1.515835458 1.544870769 1.554626219 1.56438167 1.567787243 1.567983108 1.56798815 1.567988175 1.567987937 1.567987818 1.5679877 1.5679874];

mfr_4(:,4)=[0.6 0.9 1.147136885 1.269120116 1.391103348 1.441876464 1.49264958 1.522823868 1.537911011 1.552998155 1.560880068 1.568761982 1.569725013 1.570688044 1.570763764 1.570763562 1.570763537 1.570763 1.57076];

mfr_4(:,5)=[0.62 0.9 1.152997605 1.271711074 1.390424543 1.442384194 1.494343844 1.526162193 1.557980542 1.564772153 1.571563765 1.572107017 1.57265027 1.572652318 1.572652148 1.572652129 1.572652153 1.572652 1.572665];

mfr_4(:,6)=[0.64 0.9 1.159789706 1.392030334 1.494134091 1.540840322 1.560799962 1.560954823 1.573105069 1.573121003 1.573797048 1.573833491

1.573834099 1.573835083 1.573834946 1.57383494 1.573834947 1.5738349 1.5738345];

mfr_4(:,7)=[0.65 0.9 1.157964458 1.276686992 1.395409525 1.445102066 1.494794606 1.528386187 1.561977769 1.567868197 1.573758625 1.574069451 1.574380276 1.574381637 1.574381632 1.574381542 1.574381537 1.5743815 1.5743813];

TPR(:,1)=[1.09 1.13 1.167718474 1.238963353 1.310208232 1.423186246 1.592155072 1.726265841 1.809694019 1.855176997 1.855694553 1.885247178 1.885560656 1.93396439 1.934070742 1.873219215 1.873445106 1.874 1.875];

TPR(:,2)=[1.09 1.12 1.166510092 1.245691447 1.324872802 1.454622784 1.55350105 1.652379315 1.732478123 1.812576931 1.915658632 1.975673143 2.01563281 2.016082469 2.065576765 2.002520235 2.002518286 2.001 2];

TPR(:,3)=[1.085 1.12 1.159665832 1.245338589 1.331011347 1.403427257 1.475843168 1.589177855 1.702512543 1.796693568 1.890874593 2.015219068 2.089520652 2.143079061 2.143723422 2.184455788 2.125077909 2.11 2.09];

TPR(:,4)=[1.08 1.1 1.147971595 1.238780094 1.329588593 1.408271503 1.486954414 1.614265261 1.677920685 1.741576109 1.850574669 1.959573229 2.032530356 2.105487483 2.262801173 2.309303806 2.238615935 2.22 2.2108];

TPR(:,5)=[1.08 1.1 1.131503346 1.226411508 1.321319671 1.404970089 1.488620506 1.628866903 1.7691133 1.89291012 2.01670694 2.154138345 2.291569751 2.371105815 2.399654028 2.361669509 2.340752225 2.33 2.3207];

TPR(:,6)=[1.08 1.09 1.110219976 1.307046122 1.482514973 1.640681429 1.782199589 1.783883603 2.059609879 2.061027664 2.250135665 2.375729535 2.463325283 2.464113539 2.489917491 2.431431206 2.427913762 2.425 2.423];

TPR(:,7)=[1.07 1.075 1.085288425 1.186278238 1.287268052 1.378089481 1.46891091 1.628536385 1.78816186 1.940244592 2.092327325 2.267653987 2.44298065 2.53993107 2.540774232 2.559655918 2.504771483 2.49 2.485];

```
eff_tr(:,1)=[0.9 0.885 0.858699103 0.831322444 0.803945784 0.776802091 0.751120365 0.746351798 0.750619307 0.764342039 0.763694562 0.768155149 0.768117576 0.746390745 0.747866652 0.781128058 0.781082222 0.7809 0.7805];

eff_tr(:,2)=[0.9 0.895 0.881945184 0.863166558 0.844387932 0.815724832 0.803414761 0.791104689 0.789465271 0.787825853 0.792311596 0.802934642 0.804603617 0.804518149 0.783729898 0.815971873 0.815975207 0.815976 0.81598];

eff_tr(:,3)=[0.897 0.895 0.88781211 0.880732968 0.873653826 0.861368784 0.849083743 0.836073829 0.823063915 0.821714624 0.820365333 0.824723222 0.832628237 0.830327339 0.830147454 0.815266395 0.842603401 0.845 0.846];

eff_tr(:,4)=[0.875 0.878 0.880832454 0.885015813 0.889199171 0.881906929 0.874614687 0.862095127 0.855835347 0.849575567 0.848031583 0.8464876 0.84845181 0.850416019 0.849896519 0.834215379 0.863498737 0.865 0.867];

eff_tr(:,5)=[0.785 0.817 0.851632598 0.873320529 0.89500846 0.892588732 0.890169004 0.880721929 0.871274853 0.869202824 0.867130796 0.870103222 0.873075649 0.865275214 0.856364468 0.871525114 0.879916571 0.882 0.885];

eff_tr(:,6)=[0.59 0.68 0.784324623 0.894567673 0.897161852 0.893587167 0.888042435 0.887813819 0.883529395 0.883526473 0.885359685 0.885964285 0.877430142 0.877222405 0.869858215 0.892067064 0.893494464 0.894 0.895];

eff_tr(:,7)=[0.3 0.45 0.640283596 0.762519588 0.884755579 0.892075764 0.899395949 0.898485459 0.897574969 0.89602263 0.894470291 0.894958003 0.895445715 0.886252953 0.886042622 0.881911397 0.90214979 0.903 0.9035];

N(1:19,1)=30000;

N(1:19,2)=35000;

N(1:19,3)=40000;

N(1:19,4)=50000;

N(1:19,5)=55500;
```

```
N(1:19,6)=61500;

N(1:19,7)=65000;

match_N = [30000; 35000; 40000; 50000; 55500; 61500; 65000];

R=287;      %J/kgK

Q_fuel=42000000;

Tmax=970;

Tmatch=1344;

Pt_std=98500; % Or 101325 for land

Tt_std=298; % Or 288.15 for land

PL_in=0.01; %Intake Pressure Loss

PL_cc=0.05; %Combustion chamber Pressure Loss

PL=[1       2];

PL_c=PL(1)/100;  %Cold Pressure Loss

PL_h=PL(2)/100; %Hot Pressure Loss

%% Inlet Temperatures

Tt2=Tt_std;

Tt4=Tmax;

%% Pressures

Pt2=Pt_std-Pt_std*PL_in;

Pt3=CPR*Pt2;
```

```
Pt3x= Pt3-PL_c*Pt3;

Pt4=Pt3x-Pt3x*PL_cc;

teta_c= (Tt2/Tt_std)^0.5;

teta_match= (Tmatch/Tt_std)^0.5;

teta_t=(Tmax/Tt_std)^0.5;

delta_c=Pt2/Pt_std;

delta_t=Pt4/Pt_std;

%% Outlet Temperatures

cp=@(T) 4.09341213523171E-18*T^6 - 2.08388586062245E-14*T^5 + 1.60579075500011E-10*T^4 - 6.00680935166874E-07*T^3 + 9.09723014905150E-04*T^2 - 3.55845026050783E-01*T + 1.04674396962907E+03;

cp_c=cp(Tt2); %compressor cp

cp_t=cp(Tt4); %turbine cp

cp_ave=(cp_c+cp_t)/2;

k_c=cp_c/(cp_c-R);

k_t=cp_t/(cp_t-R);

Tt3s=Tt2*(CPR.^((k_c-1)/k_c)); %compressor outlet_ideal

Tt3a=Tt2+((Tt3s-Tt2)./eff_co); %compressor outlet_actual

Tt3x=Tt3a+TR;   %Temperature Rise in Recuperator

Tt5s = Tt4./(TPR.^((k_t-1)/k_t));   %turbine outlet_ideal

Tt5a = Tt4-(eff_tr.*(Tt4-Tt5s));    %turbine outlet_actual
```

```
Tt5x=Tt5a-TR;   %Temperature Rise in Recuperator

%% Corrected Mass Flow Rate

m_fuel = mfr_2.*cp_ave.*(Tt4-Tt3x)/Q_fuel;

f = m_fuel./mfr_2;

corr_mfr2= (1+f).*(1./(Pt4/Pt2)).*((mfr_2.*N)./(delta_c))*(Tmatch/Tmax)^0.5;

corr_mfr4= (mfr_4*teta_match./delta_t).*N./teta_t;

N_c        = N./teta_c;

N_t        = N./teta_t;

%% Corrected Entalpy

deltaH_c = cp_c.*(Tt3a-Tt2);

deltaH_t = cp_t.*(Tt4-Tt5a);

corr_deltaH_c= deltaH_c./((1+f).*(N.^2));

corr_deltaH_t= deltaH_t./(N.^2);

%% Finding Intersection Points

Intersect_1 = InterX([corr_mfr2(:,1) corr_deltaH_c(:,1)]',[corr_mfr4(:,1) corr_deltaH_t(:,1)]') ;

Intersect_2 = InterX([corr_mfr2(:,2) corr_deltaH_c(:,2)]',[corr_mfr4(:,2) corr_deltaH_t(:,2)]') ;

Intersect_3 = InterX([corr_mfr2(:,3) corr_deltaH_c(:,3)]',[corr_mfr4(:,3) corr_deltaH_t(:,3)]') ;

Intersect_4 = InterX([corr_mfr2(:,4) corr_deltaH_c(:,4)]',[corr_mfr4(:,4) corr_deltaH_t(:,4)]') ;
```

Intersect_5 = InterX([corr_mfr2(:,5) corr_deltaH_c(:,5)]',[corr_mfr4(:,5) corr_deltaH_t(:,5)]') ;

Intersect_6 = InterX([corr_mfr2(:,6) corr_deltaH_c(:,6)]',[corr_mfr4(:,6) corr_deltaH_t(:,6)]') ;

Intersect_7 = InterX([corr_mfr2(:,7) corr_deltaH_c(:,7)]',[corr_mfr4(:,7) corr_deltaH_t(:,7)]') ;

Intersect=[Intersect_1 Intersect_2 Intersect_3 Intersect_4 Intersect_5 Intersect_6 Intersect_7];

%% % AFTER MATCHING % %%

match_corr_mfr = Intersect(1,:).' ;

match_corr_deltaH = Intersect(2,:).';

%% Physical Enthalpy Calculaion

match_deltaH_c= match_corr_deltaH.*((1+initial_f).*(match_N.^2)); %physical enthalpy comp

match_deltaH_t= match_corr_deltaH.*match_N.^2; %physical enthalpy turb

match_CPR=[interp1(deltaH_c(:,1),CPR(:,1),match_deltaH_c(1));interp1(deltaH_c(:,2),CPR(:,2),match_deltaH_c(2));interp1(deltaH_c(:,3),CPR(:,3),match_deltaH_c(3));interp1(deltaH_c(:,4),CPR(:,4),match_deltaH_c(4));interp1(deltaH_c(:,5),CPR(:,5),match_deltaH_c(5));interp1(deltaH_c(:,6),CPR(:,6),match_deltaH_c(6));interp1(deltaH_c(:,7),CPR(:,7),match_deltaH_c(7))];

match_TPR=[interp1(deltaH_t(:,1),TPR(:,1),match_deltaH_t(1));interp1(deltaH_t(:,2),TPR(:,2),match_deltaH_t(2));interp1(deltaH_t(:,3),TPR(:,3),match_deltaH_t(3));interp1(deltaH_t(:,4),TPR(:,4),match_deltaH_t(4));interp1(deltaH_t(:,5),TPR(:,5),match_deltaH_t(5));interp1(deltaH_t(:,6),TPR(:,6),match_deltaH_t(6));interp1(deltaH_t(:,7),TPR(:,7),match_deltaH_t(7))];

match_eff_co=[interp1(deltaH_c(:,1),eff_co(:,1),match_deltaH_c(1));interp1(deltaH_c(:,2),eff_co(:,2),match_deltaH_c(2));interp1(deltaH_c(:,3),eff_co(:,3),match_deltaH_c(3));interp1(deltaH_c(:,4),eff_co(:,4),match_deltaH_c(4));interp1(deltaH_c(:,5),eff_co(:,5),match_deltaH_c(5));interp1(deltaH_c(:,6),eff_co(:,6),match_deltaH_c(6));interp1(deltaH_c(:,7),eff_co(:,7),match_deltaH_c(7))];

match_eff_tr=[interp1(deltaH_t(:,1),eff_tr(:,1),match_deltaH_t(1));interp1(deltaH_t(:,2),eff_tr(:,2),match_deltaH_t(2));interp1(deltaH_t(:,3),eff_tr(:,3),match_deltaH_t(3));interp1(deltaH_t(:,4),eff_tr(:,4),match_deltaH_t(4));interp1(deltaH_t(:,5),eff_tr(:,5),match_deltaH_t(5));interp1(deltaH_t(:,6),eff_tr(:,6),match_deltaH_t(6));interp1(deltaH_t(:,7),eff_tr(:,7),match_deltaH_t(7))];

%% New Pressures

match_Pt2=Pt_std-Pt_std*PL_in;

match_Pt3=match_CPR*match_Pt2;

match_Pt3x=match_Pt3-match_Pt3*PL_c;

match_Pt4=match_Pt3x-match_Pt3x*PL_cc;

match_delta_c=match_Pt2/Pt_std;

match_delta_t=match_Pt4/Pt_std;

%% %% Physical Mass Flow Rates Calculaion

match_mfr_2= match_corr_mfr.*(match_Pt4/match_Pt2)*match_delta_c./((1+initial_f).*match_N*(Tmatch/Tmax)^0.5);

match_mfr_4= match_corr_mfr.*match_delta_t*teta_t./(match_N*teta_match);

%% New Temperatures

match_Tt3s = Tt2*(match_CPR.^((k_c-1)/k_c));   %compressor outlet_ideal

match_Tt3a=Tt2+((match_Tt3s-Tt2)./match_eff_co);   %compressor outlet_actual

```
match_Tt3x=match_Tt3a+TR;

match_Tt5a=Tt4-((match_mfr_2.*cp_c.*(match_Tt3a-Tt2))./(match_mfr_4.*cp_t));
%turbine outlet_actual

match_Tt5s=Tt4-((Tt4-match_Tt5a)./match_eff_tr);    %turbine outlet_ideal

match_Tt5x=match_Tt5a+TR;

%% New Turbine Outlet Pressure

match_Pt5=match_Pt4.*(match_Tt5s./Tt4).^(k_t/(k_t-1));

match_Pt5x=match_Pt5-match_Pt5*PL_h;

%% New Fuel Mass Flow Rate and f

match_m_fuel = match_mfr_2.*((cp_c+cp_t)./2).*(Tt4-match_Tt3x)/Q_fuel;

match_f = match_m_fuel./match_mfr_2;

%% Output Parameters

Mach=(((match_Pt5x/Pt_std).^((k_t-1)/k_t)-1).*(2/(k_t-1))).^0.5;

Ts5=match_Tt5x./exp((R/cp_t).*log(match_Pt5x/Pt_std)); %Static Temperature !!!

a=(k_t*R*Ts5).^0.5;                              %Speed of Sound

V_jet=Mach.*a;

rho_s=Pt_std./(Ts5*R);                            %Static density

Pt9=Pt_std.*(1+(((k_t-1)/2).*(0.2).^2)).^(k_t/(k_t-1));

Tt9=match_Tt5x.*((Pt9./match_Pt5x).^((k_t-1)./k_t));

Thrust=(match_mfr_2+match_m_fuel).*V_jet;

A_jet=match_mfr_2./(V_jet.*rho_s);

D_jet=(A_jet/pi).^0.5;
```

```
SFC=match_m_fuel./Thrust;                    %Specific Fuel Consumption

digitsOld = digits(20);

SFC = vpa(SFC(6));

deltaT=Tt4-match_Tt3a(6)-((Q_fuel*V_jet(6)*0.000027048)/(((cp_c+cp_t)/2)*(1-
(V_jet(6)*0.000027048)))); % 0.000027048 is SFC of simpcle cycle

epsilon = 10^-6;

err1=abs(TR-deltaT);

if err1<epsilon

break

end

TR=deltaT;

end

%% Calculation of Effectiveness

Qa=(cp_c*(TR)); %actual

Qmax=(cp_c*(match_Tt5a-match_Tt3a));

EFF=Qa./Qmax;

vpa(EFF(6))

%% Calculation of Power of The Additional Turbine

W=(match_mfr_2(6)+match_m_fuel(6))*cp_t*(match_Tt5x(6)-Tt9(6))

Q=Q_fuel*match_m_fuel(6)

n=W/Q
```

Republic of Turkey

İzmir Kâtip Çelebi University

Graduate School of Natural and Applied Sciences

Exhaust Thermal Energy Recuperation in Small Gas Turbine and Turbojet Engines

Department of Mechanical Engineering

Master’s Thesis

Deniz Hakyemez Çetiner

ORCID 0000-0002-5279-9235

Thesis Advisor: Assoc. Prof. Dr. Sercan Acarer

January 2022

HAKYEMEZ ÇETİNER   Exhaust Thermal Energy Recuperation in Small Gas Turbine and Turbojet Engines   MASTER’S THESIS   2022

Curriculum Vitae

Name Surname : Deniz Hakyemez
E-mail (1) : denizhkymz@gmail.com

Education:

2013–2018 İzmir Kâtip Çelebi University, Dept. of Mechanical Eng.

2018–2021 İzmir Kâtip Çelebi University, Dept. of Mechanical Eng.

Work Experience:

Jul. 2017 – Aug. 2017 Intern – KLAS Heating, Refrigeration, Air-conditioning Industry and Trade Ltd.

Oct. 2018 – Feb. 2019 Sales Engineer – Dogu HVAC Systems

Feb. 2019 – Jun. 2019 R&D Engineer – Dogu HVAC Systems

Jun. 2019 – May. 2021 Researcher – NATO Science for Peace and Security (SPS) Program

Publications (if any):

1. Hakyemez Deniz, Yıldırım Cansu, Acarer Sercan, Preliminary Design Optimization of a Recuperator for a Micro Turbojet Engine and Its Impact on The Engine Performance, TESKON 2019,17.04.2019 20.04.2019, Izmir, Turkey (http://mmoteskon.org/wp-content/uploads/2019/03/2019-073.pdf)
2. Hakyemez Deniz, Acarer Sercan, Accurately Capturing Heat Transfer in a Turbulent U-Bend Flow, 4th International Students Science Congress page 424, 18.09.2020 19.09.2020, Izmir, Turkey